

Magnetic fields in the cores of Taurus/B213
from JCMT BISTRO survey
(preliminary results)

Eswaraiah Chakali
(FAST fellow, NAOC, China)

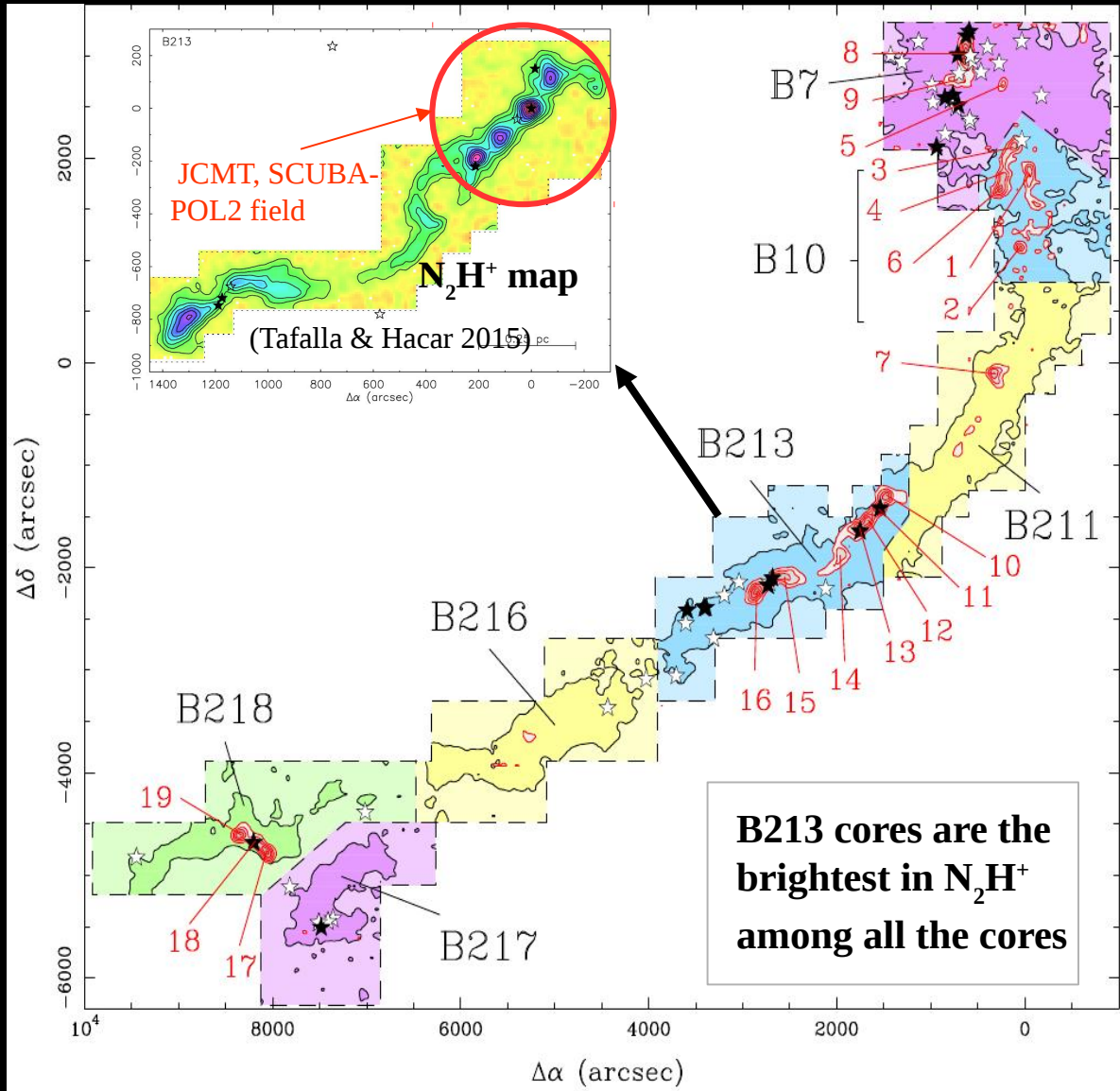
Prof. Di Li
(NAOC, China)

Collaborators

Keping Qiu, Tao-Chung Ching, Shih-Ping Lai, Jia-Wei Wang, Tie Liu

and
BISTRO team

LDN1495/B213 in Taurus



→ L1495/B213 is one of the most prominent filaments in nearby clouds in Gould belt.

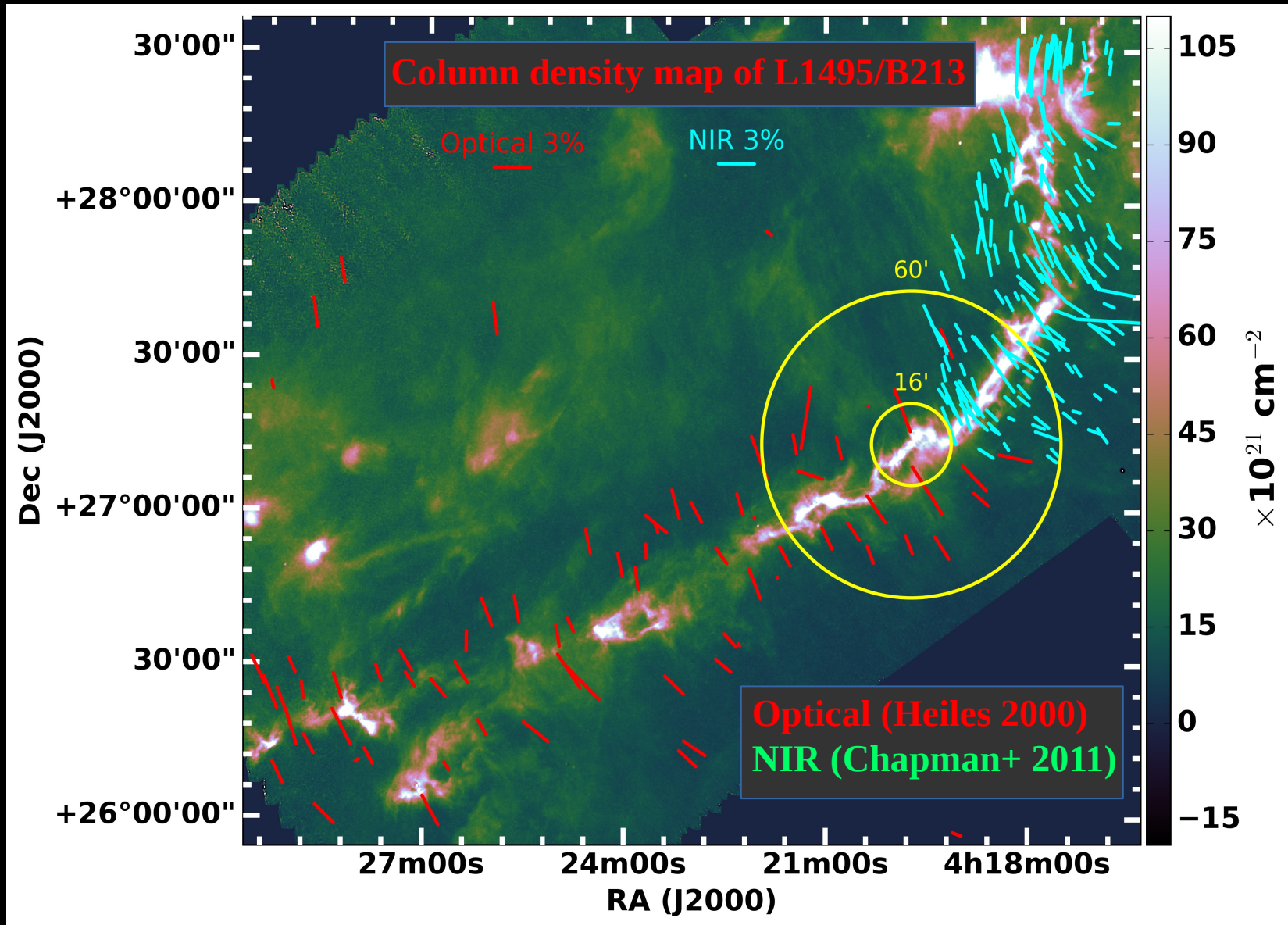
- well-studied
- Length ~ 10 pc
- Mass $> 700 M_{\text{sun}}$
- ~ 40 YSOs,
- ~ 20 dense cores

(Hacar & Tafalla 2011, Hacar+ 2013)

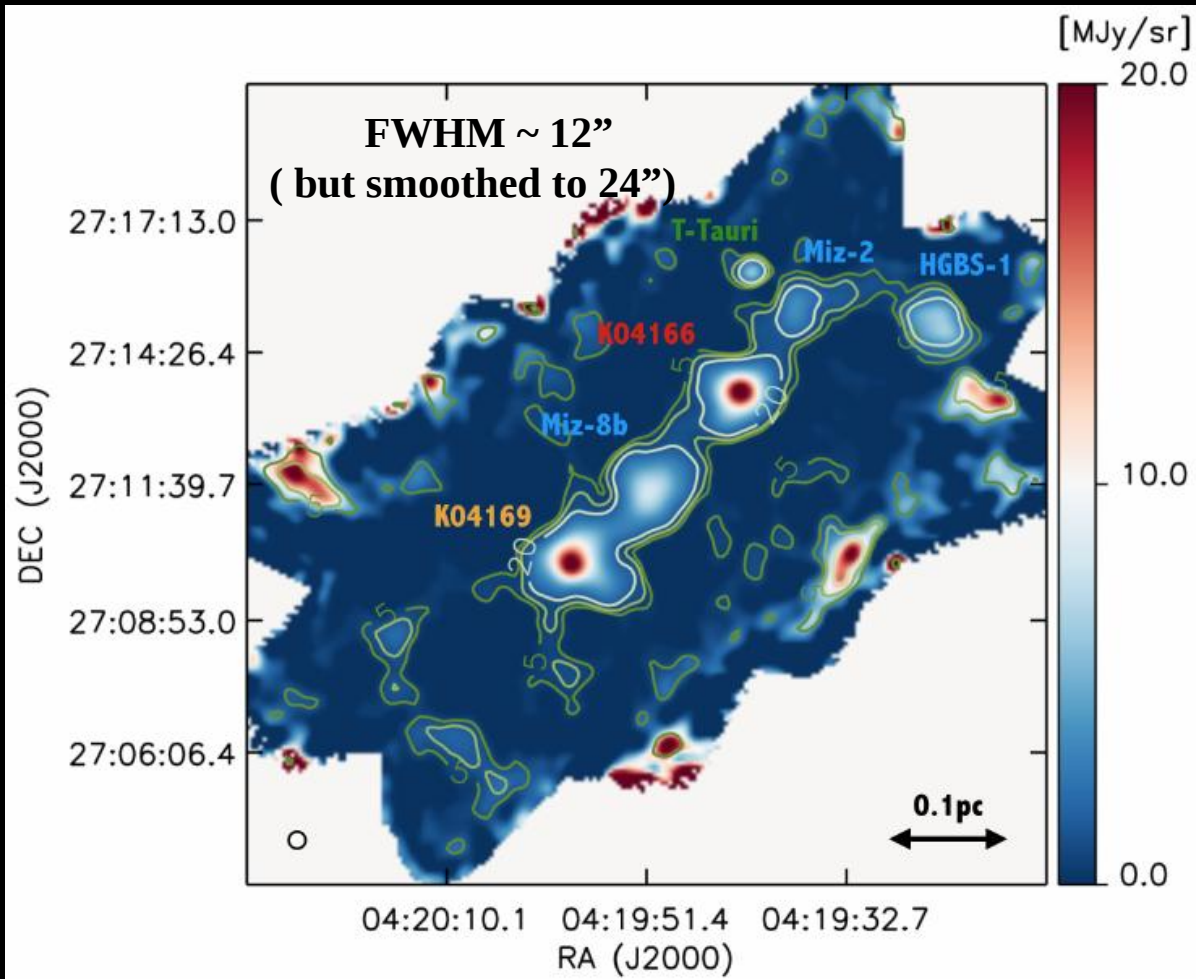
→ **Agents governing the connection between low density ISM, filaments, cores, and star formation in them?**

Distribution of regions and their cores. $C^{18}O$ (black contour: 0.5 K km/s) and N_2H^+ (red contour: N_2H^+). Solid & open stars: Class I/Flat & Class II/III (Rebull+ 2010). Distance ~ 130 pc (Dzib+ 2019)

B-fields at larger scales based on optical and NIR polarimetry



At $\sim \text{pc}$ to $\sim \text{several pc}$ scales B-fields are organized; either perpendicular to the dense filaments or aligned parallel to the low density striations. SCUBA-POL2 FOV: 16' diameter. Column density map is from Gould belt Survey (Palmeirim+ 2013; <http://gouldbelt-herschel.cea.fr/archives>)



B213 NW filament and its hierarchically fragmented chain of cores

- Dust continuum map at 1.15 mm with NIKA camera of IRAM-30 m telescope

(Bracco+ 2017)

3 prestellar and 3 protostellar

Object	Evolutionary stage	RA (J2000)	Dec (J2000)	Abbreviation in text and figures
HGBS-J041937.7+271526 ^{a,e}	Prestellar	04 ^h 19 ^m 37.7 ^s	+27°15'20.0''	Miz-2
HGBS-J041923.9+271453 ^e	Prestellar	04 ^h 19 ^m 23.9 ^s	+27°14'53.0''	HGBS-1
Miz-8b ^{a,c}	Prestellar	04 ^h 19 ^m 51.0 ^s	+27°11'42.2''	Miz-8b
K04166 ^b	Class 0/I	04 ^h 19 ^m 42.9 ^s	+27°13'38.8''	K04166
K04169 ^b	Class 0/I	04 ^h 19 ^m 58.9 ^s	+27°10'00.5''	K04169
J04194148+2716070 ^d	T Tauri	04 ^h 19 ^m 41.5 ^s	+27°16'07.0''	T Tauri

Log of observations

Log of observations: date, number of sets acquired, sequence number, and atmospheric opacity.

Date of observation	No. of sets	Sequence number	τ	
2018 Nov 23	3	40,41,45	0.04,0.04,0.04	
2018 Nov 25	3	51,53,58	0.05,0.06,0.06	
2018 Dec 03	2	32,39	0.05,0.05	
2018 Dec 06	4	18,22,28,44	0.04,0.03,0.05,0.05	
2018 Dec 11	2	45,48	0.02,0.2	
2018 Dec 21	1	48	0.03	Tau < 0.07
2018 Dec 23	1	44	0.05	Band 1 & 2
2019 Jan 03	1	18	0.05	weather
2019 Jan 04	2	10,14	0.04,0.04	
2019 Jan 08	1	11	0.04	

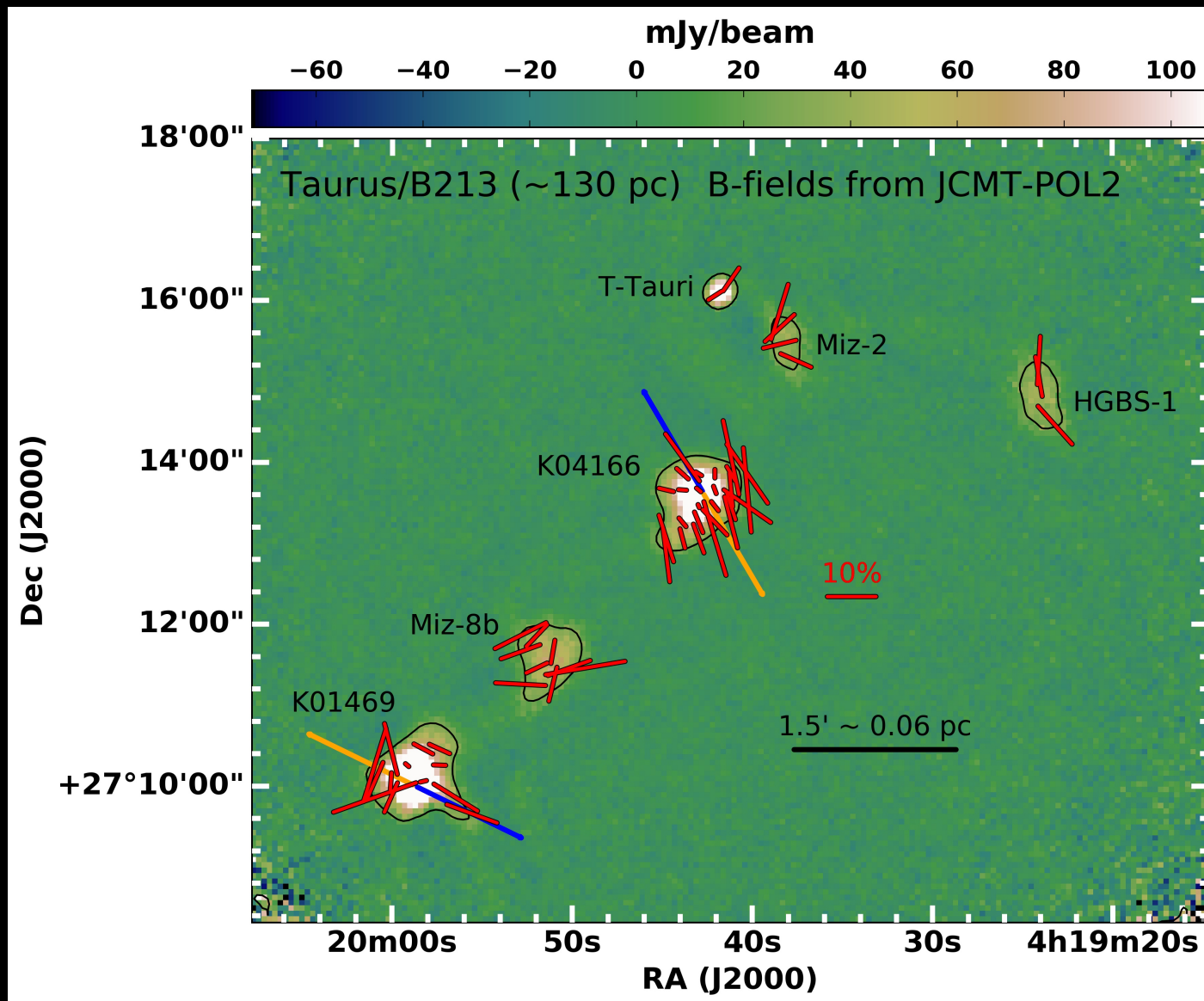
Total 20 sets were acquired with a total observing time of ~14.1 hrs

Recent (04 April 2019) pol2map is used

POL2MAP: options in steps 1, 2, and 3: NNNY, YYNY, YYNY
(skyloop, mapvar, normalise, obsweight)

Two sets (#40 and #41) acquired on 2018 Nov 23 are given lowest weight and are excluded by pol2map; therefore **18 sets used to produce final results**

B-field geometry in the cores of B213 based on JCMT/SCUBAPOL2

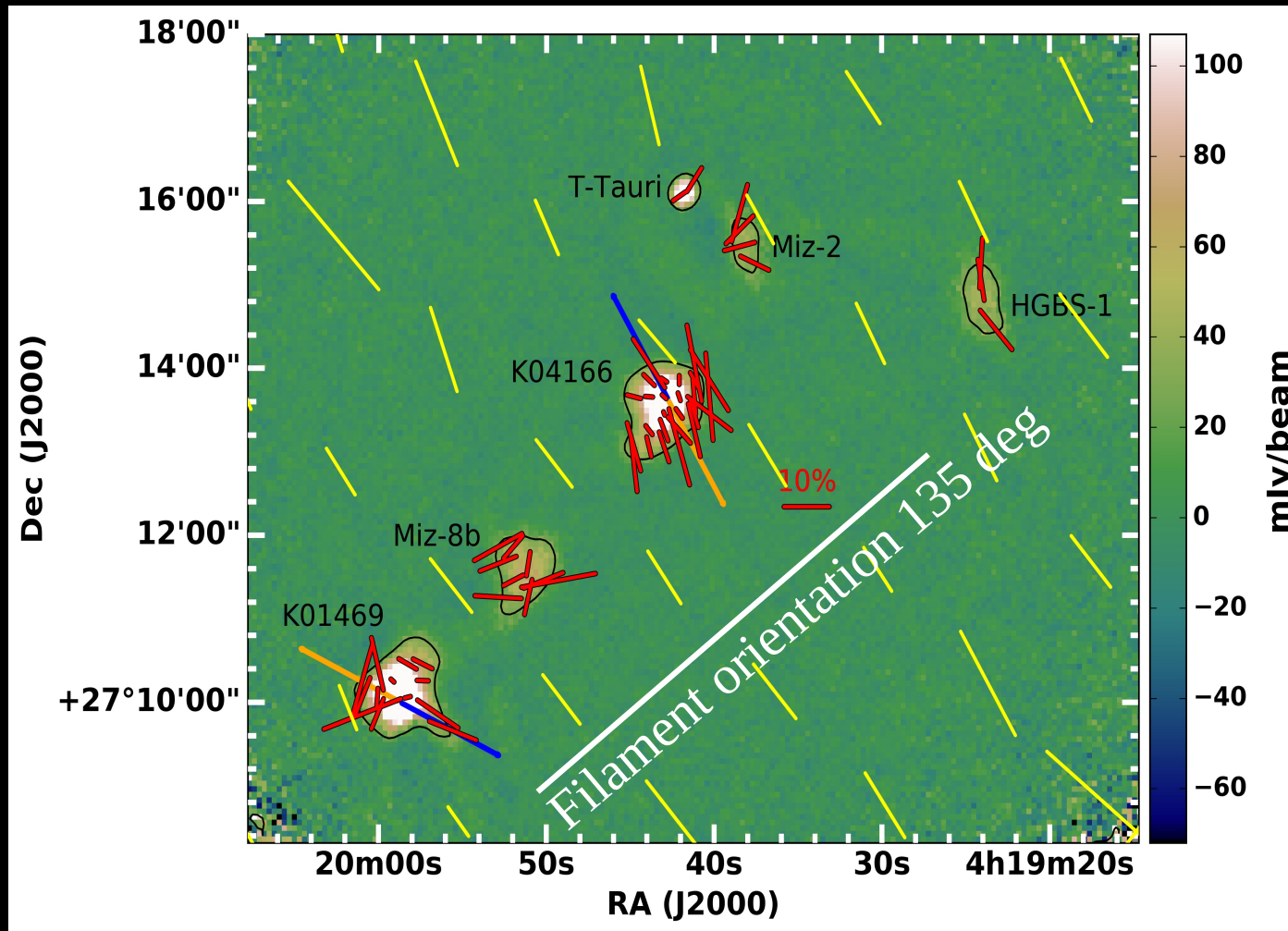


Rms noise: 5 mJy/beam, pixel size = 4", vector map binned over 12 arcsec

Data selection: $P/DP > 2$, $I/DI > 10$, $P < 30\%$

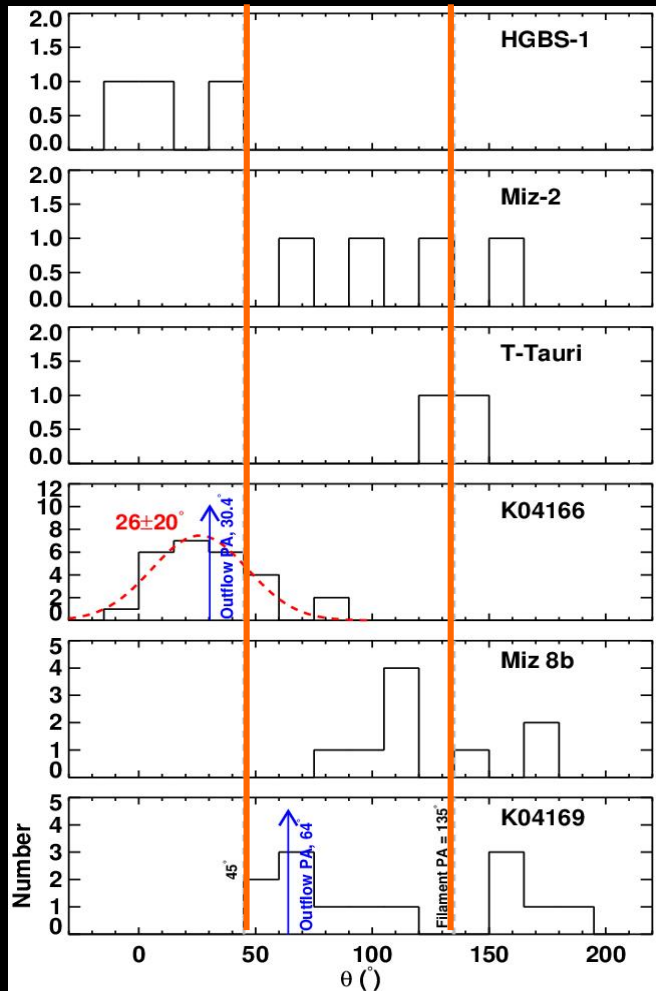
Background image: POL2 Stokes I map, black contour at 25 mJy/beam

Comparison between B-fields at larger and smaller scales



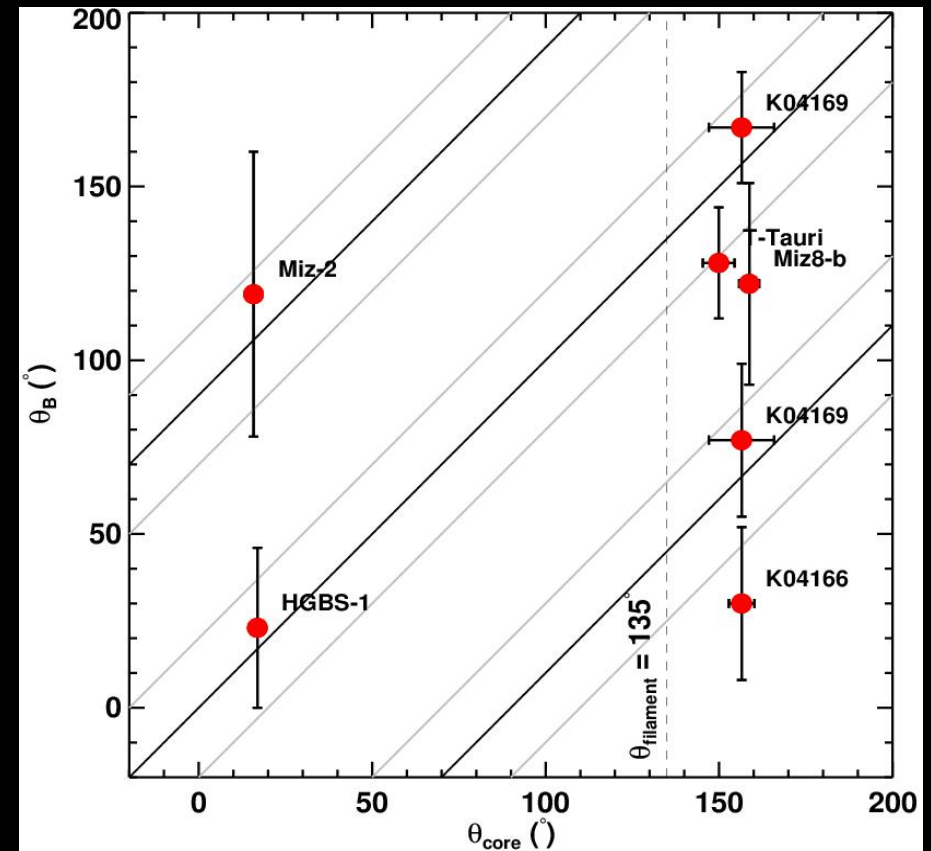
Absence of coherency between Optical/NIR/Planck and JCMT/SCUBAPOL2 B-fields. However, B-fields in HGBS-1, K01466, k04169 are coherent with large scales B-fields, while in Miz-2, Miz-8b, and T-Tauri they are perpendicular.

B-fields vs PA of filament



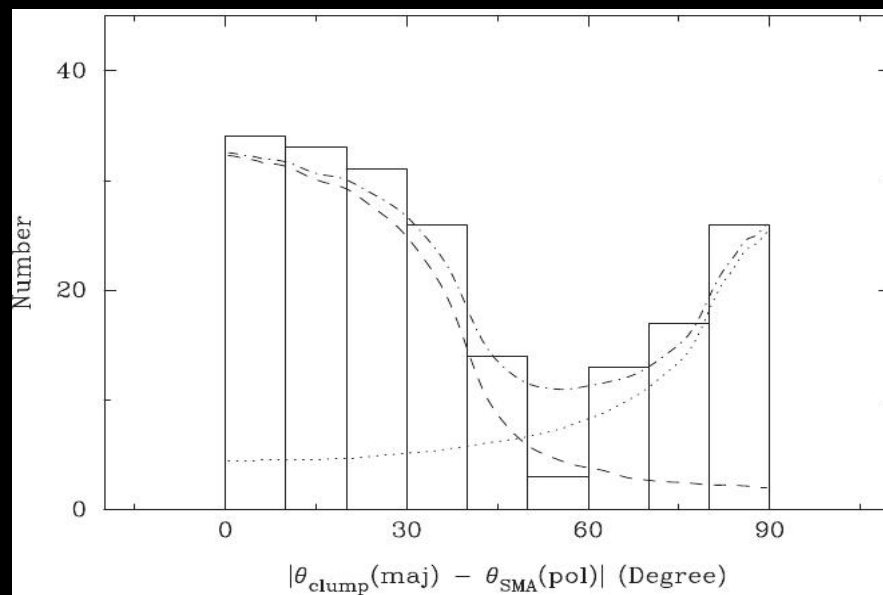
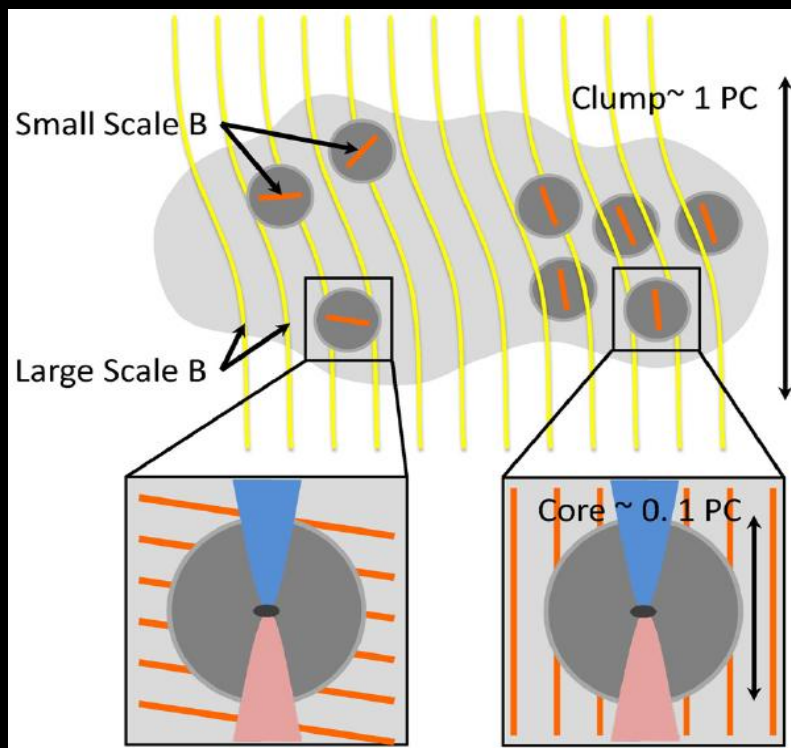
B-fields at cores scales are either parallel or perpendicular to the filament long axis (and also to the larger scale B-fields)

B-fields vs PA of the cores



Major axes of the cores are either parallel or perpendicular to their mean B-field geometries
==> Bimodal distribution at larger and smaller scales

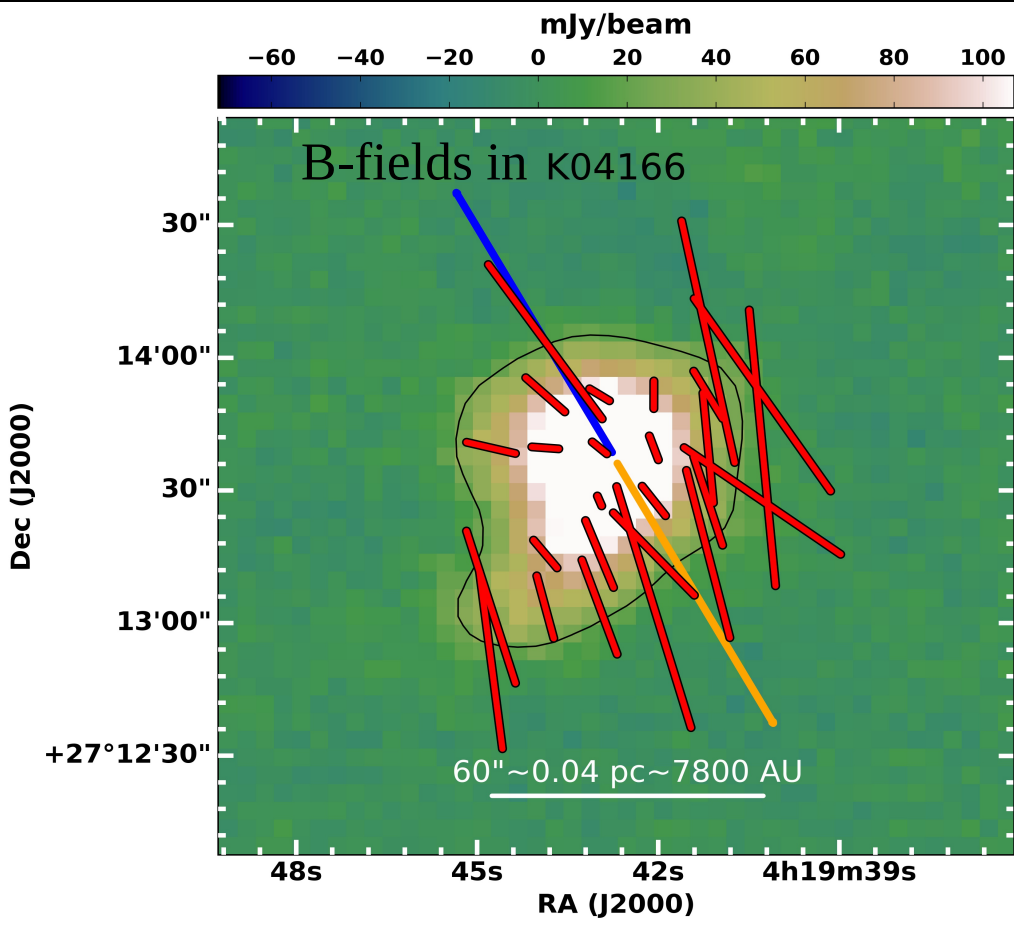
Correlation between the morphologies of B-fields and cores (other studies)



**B-fields vs core geometries in 14 different massive clumps, bimodal distribution,
(based on SMA data, Zhang+ 2014)**

B-fields at pc and sub-pc scales are either parallel and/or perpendicular to the core geometries in massive star forming cores indicating the importance of B-fields.

Magnetically dominated star formation in K04166?



Mean B-fields at various scales

Optical 29 ± 14 deg

NIR 37 ± 17 deg

Planck 29 ± 17 deg

JCMT-POL2 26 ± 20 deg

Outflow PA 30 deg

Magnetically regulated low-mass star formation via ambipolar diffusion?

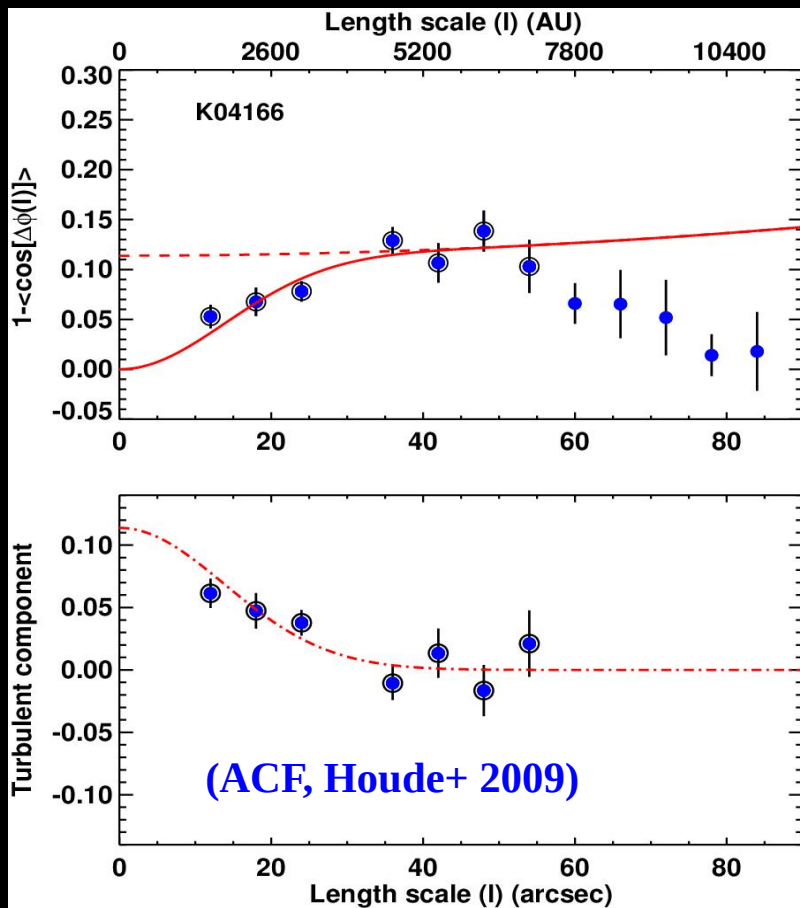
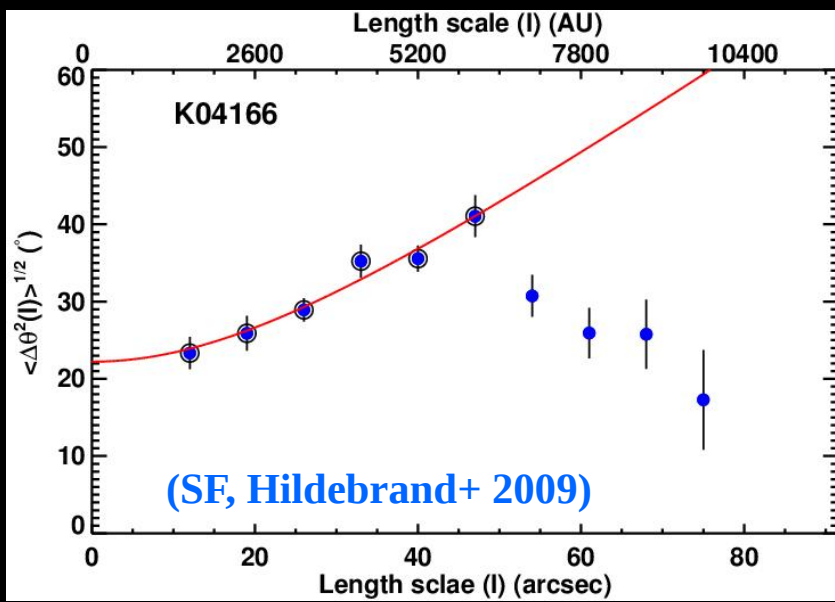
Hour-glass B-fields?

B-field strength using DCF relation, magnetic criticality parameter

sno	Parameter	Value
1	Column density $N(\text{H}_2)$ (10^{21} cm^{-2})	22 ± 6
2	Effective radius (R_{eff} ; arcsec)	10.96 ± 0.08
3	Number density $n(\text{H}_2)$ ($\times 10^5$) (cm^{-3})	8.27 ± 0.17
4	Mass (M_\odot)	0.08
5	Gas velocity dispersion ($\sigma_{V_{LSR}}$, km/s, from N_2H^+)	0.119 ± 0.024
6	Kinetic temperature (T_{kin} , K, from NH_3) ^c	10.39 ± 0.52
7	Thermal velocity dispersion σ_T (km/s)	0.055 ± 0.012
8	Non-thermal velocity dispersion σ_{NT} (km/s)	0.106 ± 0.027
9	Angular dispersion in θ_B (degree; Gaussian fit)	20 ± 2

sno	Parameter	Value
From Davis-Chandrasekhar-Fermi (DCF) method		
1	B-field strength (μG)	106 ± 29
2	P_B ($\times 10^{-10}$) (dyn cm^{-2})	4.5 ± 2.4
3	P_{turb} ($\times 10^{-10}$) (dyn cm^{-2})	4.3 ± 2.2
4	P_B/P_{turb}	1.0 ± 0.8
5	Magnetic criticality (μ)	1.5 ± 0.6

Structure Function and Auto-correlation Function analyses



From Structure function (SF) analysis

1	Angular dispersion (σ_θ ; degree)	22.2 ± 1.5
2	$\langle \delta B^2 \rangle^{1/2} / \langle B_o \rangle$	0.285 ± 0.019
3	B-field strength (modified DCF) (μG)	130 ± 34
4	$P_B (\times 10^{-10})$ (dyn cm^{-2})	6.6 ± 3.5
5	P_B / P_{turb}	1.5 ± 1.1
6	Magnetic criticality (μ)	1.3 ± 0.5

From Auto-correlation function (ACF) analysis

1	Angular dispersion (σ_θ)	28 ± 10
2	$\langle \delta B^2 \rangle / \langle B_o^2 \rangle$	0.17 ± 0.07
3	$(\langle \delta B^2 \rangle / \langle B_o^2 \rangle)^{1/2}$	0.41 ± 0.08
4	Turbulent correlation length (δ in arcsec)	10.9 ± 4.5
5	Coefficient (a'_2) $\times 10^{-6}$ (arcsec^2)	4 ± 19
6	B-field strength (modified DCF) (μG)	178 ± 59
7	$P_B (\times 10^{-10})$ (dyn cm^{-2})	12.6 ± 8.4
8	P_B / P_{turb}	3 ± 2
9	Magnetic criticality (μ)	0.9 ± 0.4

B-field strength: 100-180 μG

Magnetic criticality ≥ 1 and $P_B / P_{TURB} \geq 1$

K04166 \Rightarrow supercritical

Summary

- Traced B-fields in the pre/protostellar cores of B213
- Coherent and ordered B-fields at larger scales > 1 pc
- At cores scales bimodal distribution (parallel and perpendicular)
- Morphological correlation b/n B-fields, filament, and cores

Detailed analyses for K04166

- Magnetically regulated star formation?
- B-fields coherent with those of larger scales
- Outflows aligned with B-fields
- B-field strength 100-180 μG using DCF, SF, ACF analyses
- Magnetic criticality > 1 ; supercritical, core collapse
- B-field and turbulence pressures, comparable to each other
- Future observing proposals: SMA and ALMA

Observed complex B-fields – due to interaction between the supersonic converging flows, fibers, or bundles?

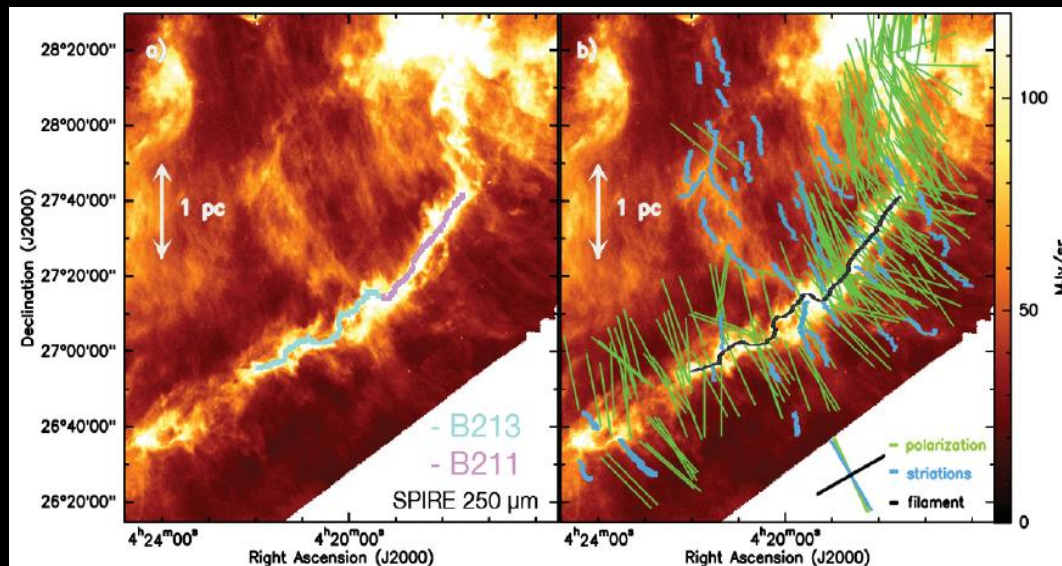
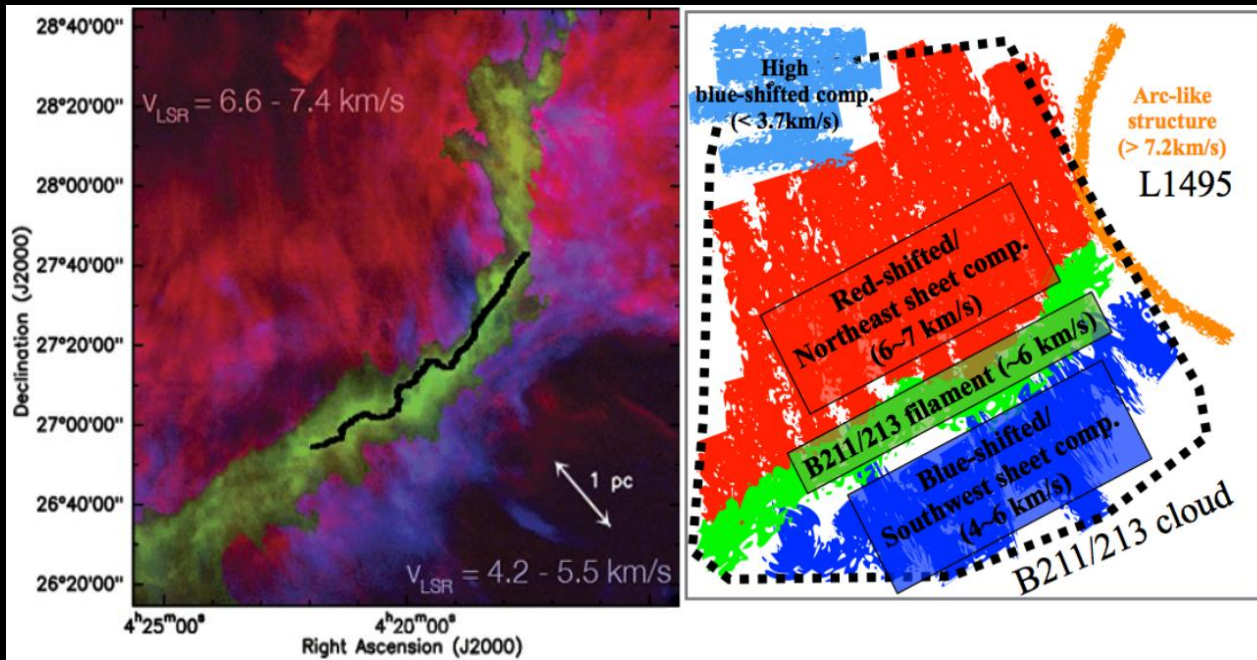
Future observations with SOFIA and SPICA-POL (B-BOP)

Eswaraiah, Li, +BISTRO team (in preparation)

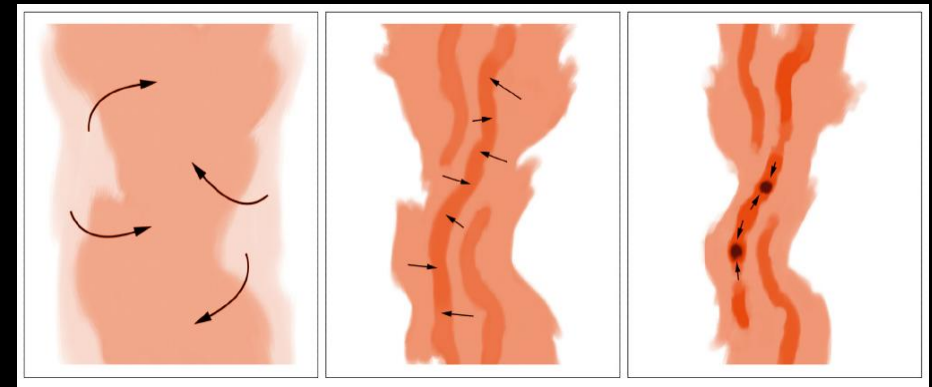
Mass accretion in B213/B211

(Left) ^{12}CO and ^{13}CO gas towards B211/B213. (Right) Schema of velocity structure.

Red: ^{12}CO , 6.6 – 7.4 km/s
 Blue: ^{12}CO , 4.2 – 5.5 km/s
 Green: ^{13}CO , 5.6 – 6.4 km/s
 (Palmeirim+ 2013, Shimijari+ 2019)

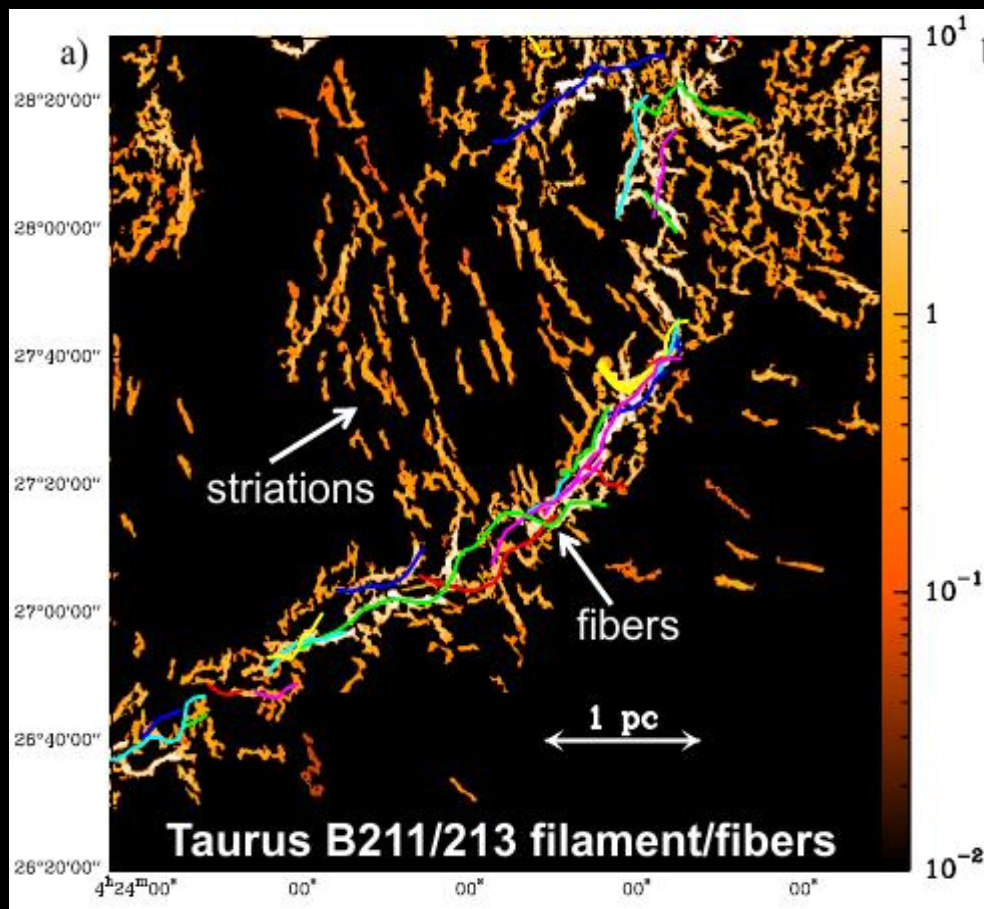


B-field guiding the material flows on to the filament, based on optical/NIR polarimetry
 (Palmeirim+ 2013, Chapman+ 2011)

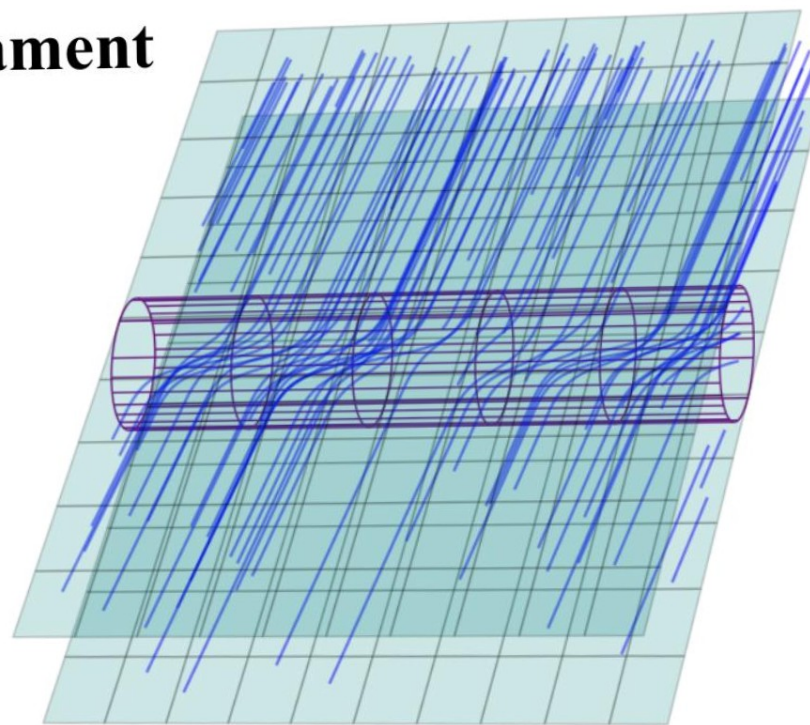


Fray and fragmentation scenario of core formation. (Left) Two colliding supersonic gas flows forming the filament. (Middle) formation of fibers due to residual turbulence and gravity. (Right) Gravitational fragmentation to form chain of cores (Tafalla & Hacar 2015).

B-fields at cores scales could more complex than those ordered B-fields at larger scales due to the interaction between fibers and gravitational compression, etc.



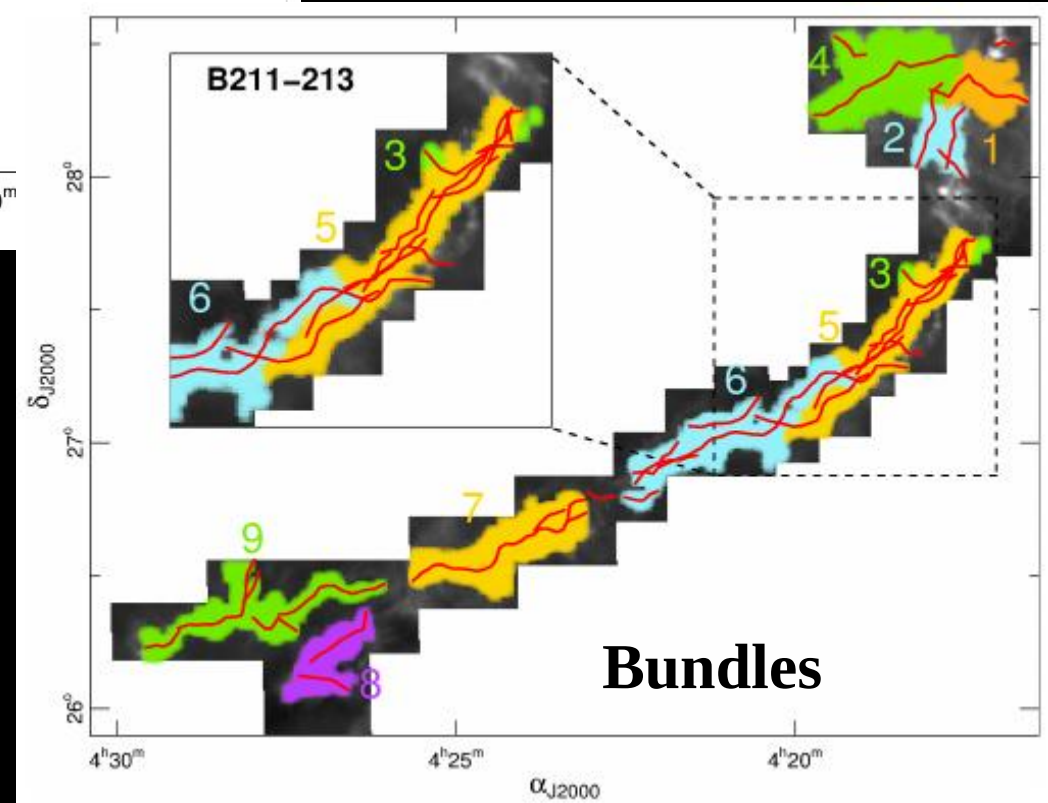
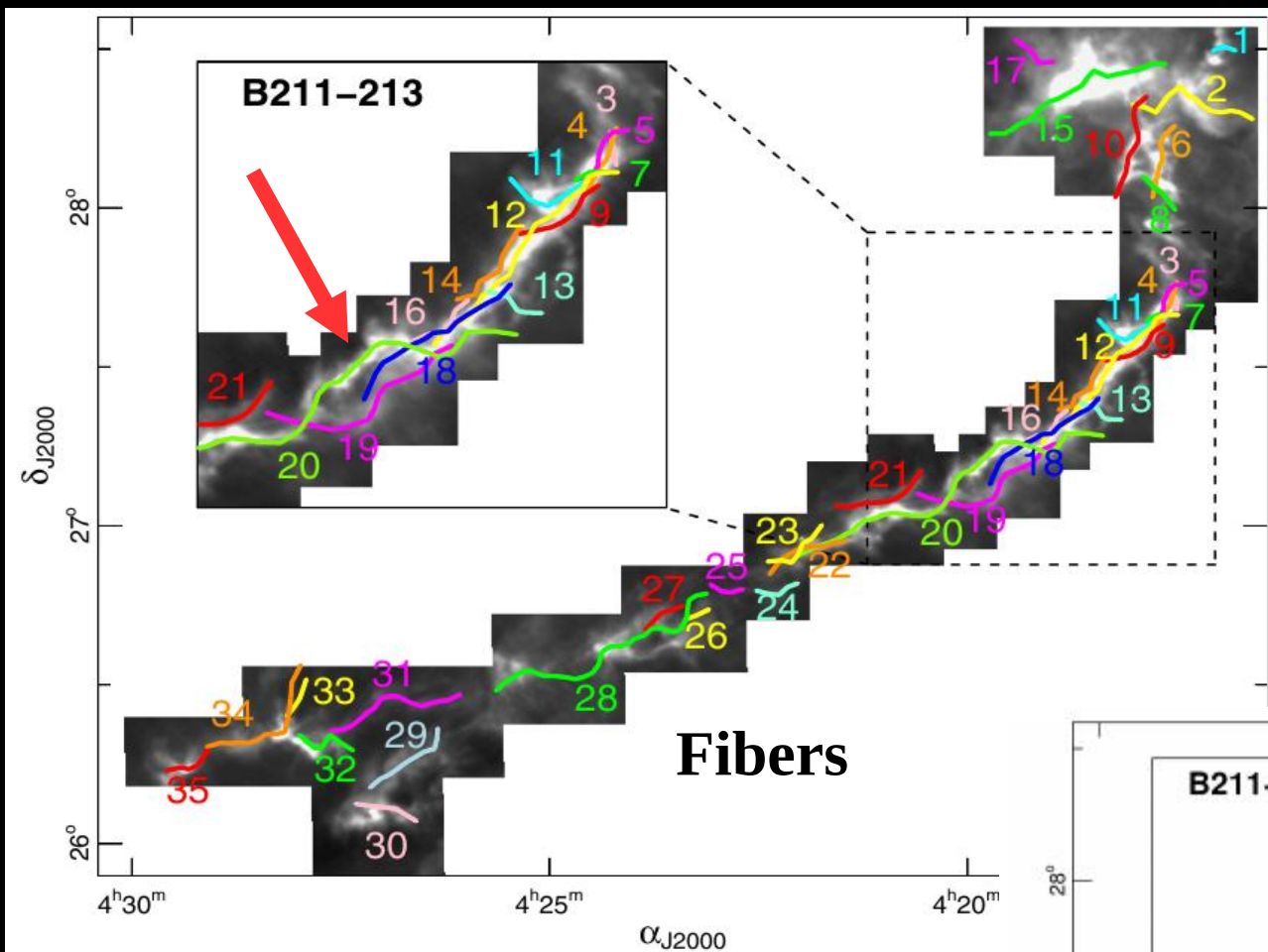
Plausible model of the B field in the central filament



B-fields perpendicular to the filament axis, and the axial component got amplified due to gravitational or turbulence compression (see Andre+ 2019, and references therein) or reorientation of oblique shocks in magnetized colliding flows (Fogerty+ 2017)

Composed of 35 network of overlapping filaments – known as fibers

- Complex kinematics
- Overlapping
- Typical length ~ 0.5 pc
- $M/L \sim 15$ Msun/pc
- Subsonic/transonic



Cores in B213 NW part are formed in the filament number '20' – which is not overlapping and interacting with adjacent fibers.

(Hacar & Tafalla 2011, Hacar+ 2013)

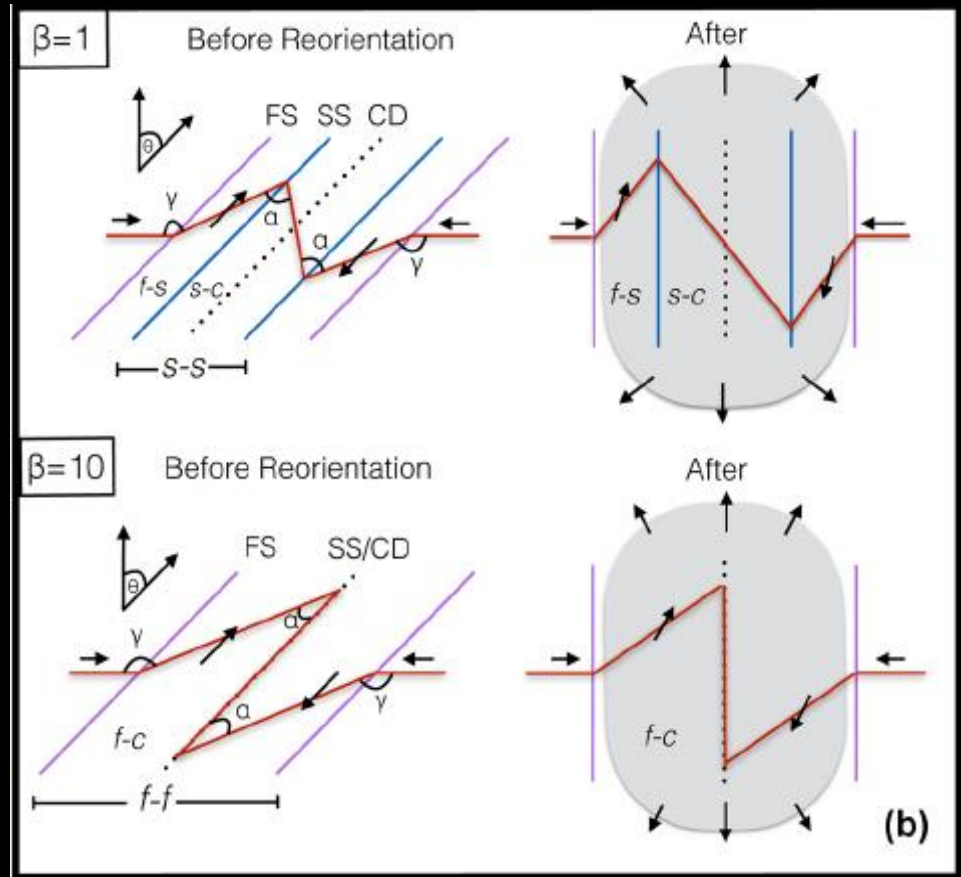
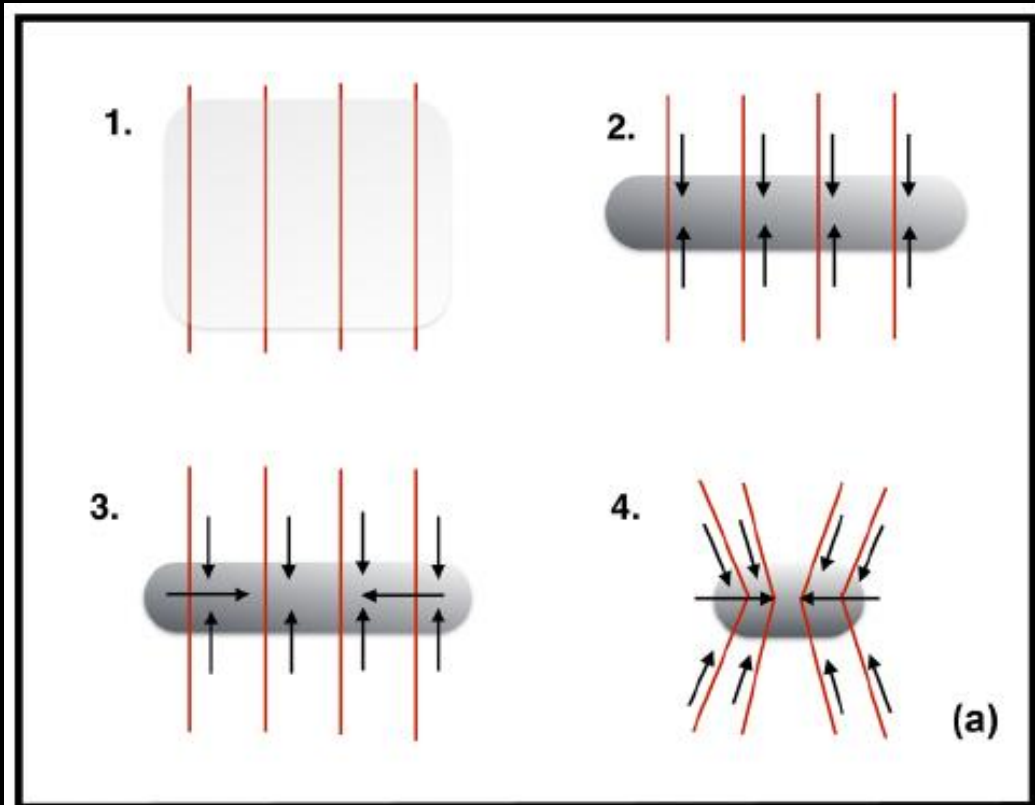
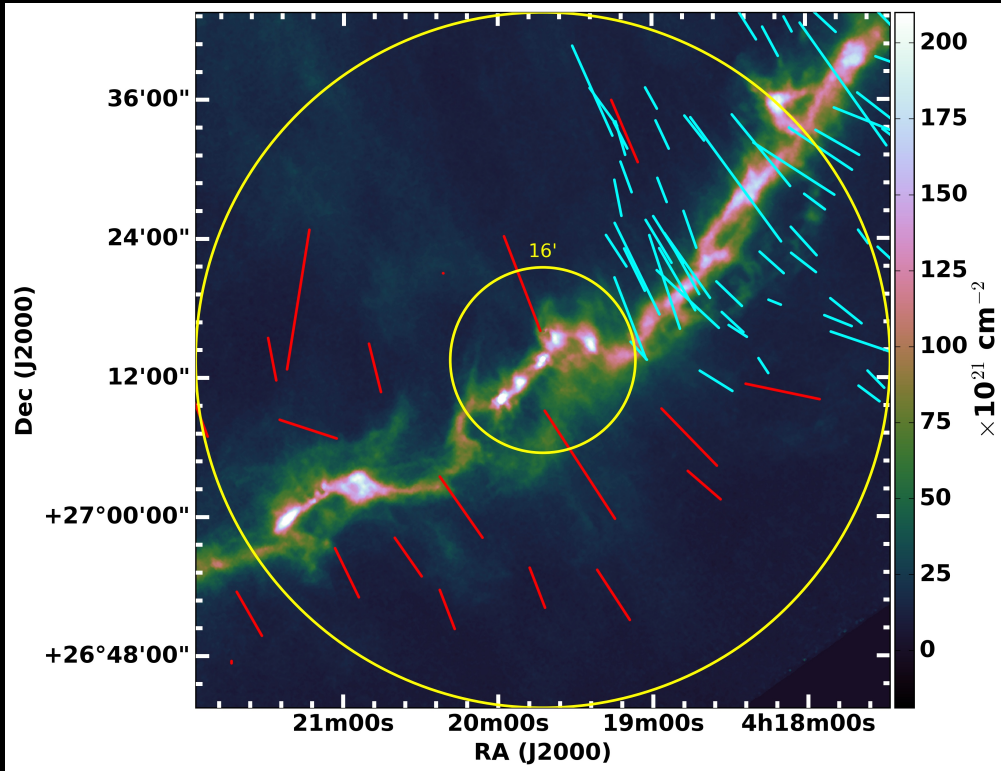


Figure 1. Mechanisms for generating filaments normal to magnetic field lines. *Top panel:* magneto-gravitational collapse. Jeans unstable gas will initially collapse along field lines (1–2). Once enough mass accumulates in the resultant filament, mass can flow along the filament and drag magnetic field lines inwards (3–4). *Bottom panel:* reorientation of magnetized oblique shocks. Uppercase letters denote wave modes, and lowercase letters give regions (see the text). Flow direction is given by the black arrows, and a representative magnetic field line is shown in red. The left-hand and right-hand panels give the initial and reoriented structures, respectively. The top and bottom rows give the moderate ($\beta = 1$) and weak field ($\beta = 10$) cases of this paper. The grey shaded region represents the growing filament.

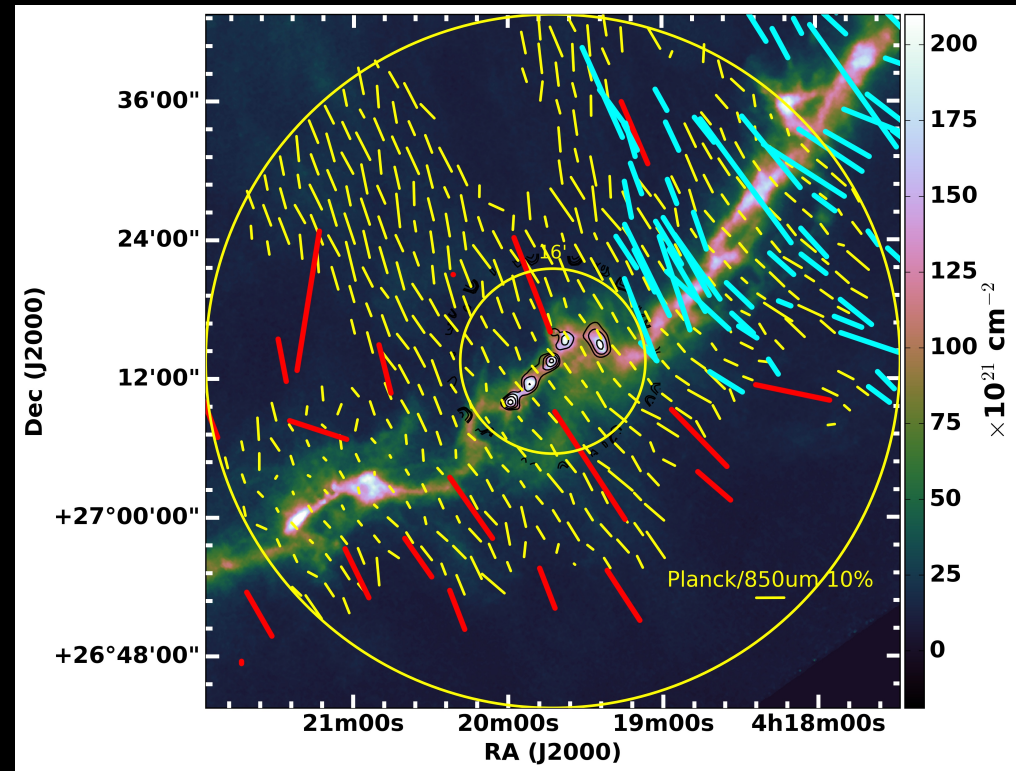
Fig 1 of Fogerty+ 2017

B-fields at pc scales

Optical + NIR



Optical + NIR + *Planck*



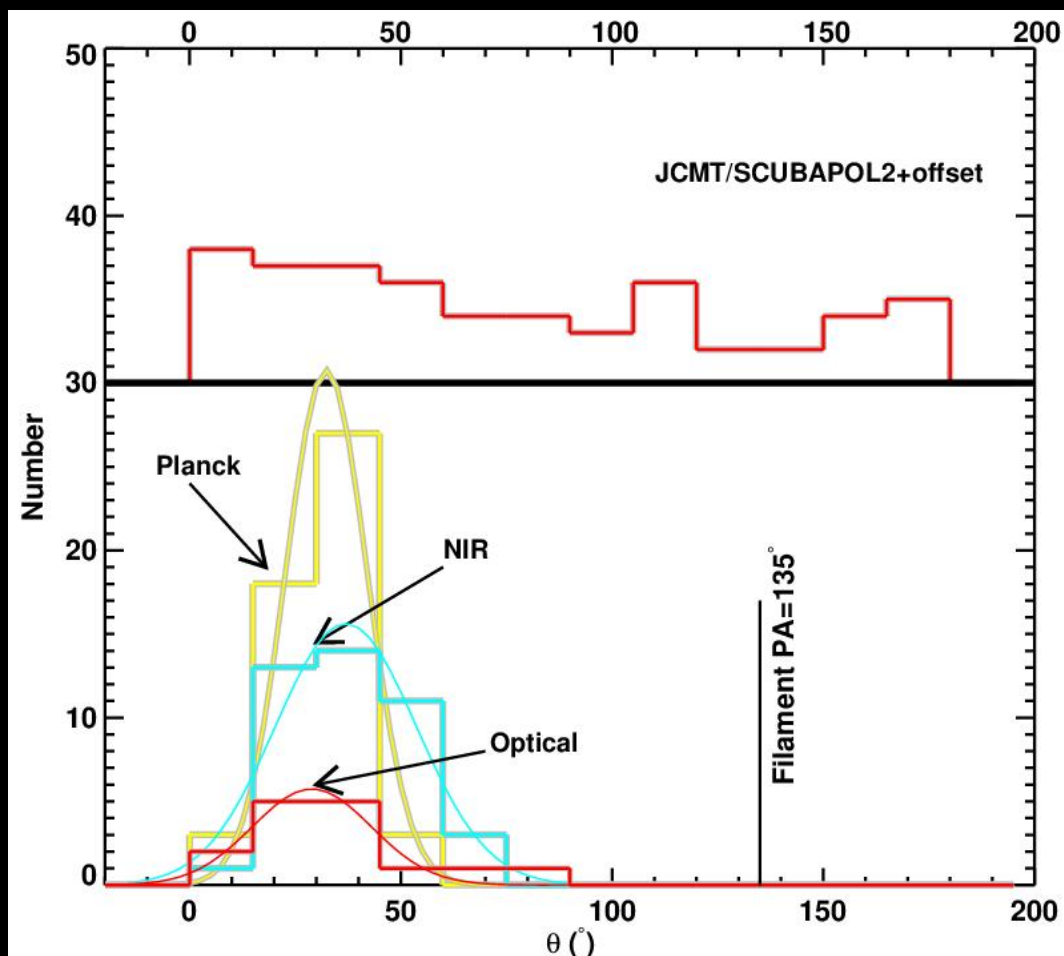
Red vectors: Optical

Cyan vectors: NIR

Yellow vectors: *Planck*/870um (for $I > 0.008 \text{ K}_{\text{CMB}}$); Resolution=5 arcmin

Background image: column density

Consistency between Optical/NIR and *Planck*/870um B-fields



B-fields at core scales (from JCMTPOL2) have mainly two components: 0 and 110 deg

Optical, NIR, and sub-mm (*Planck*) yielded mean B-fields orientations are at ~ 30 deg (4th column; Table below).

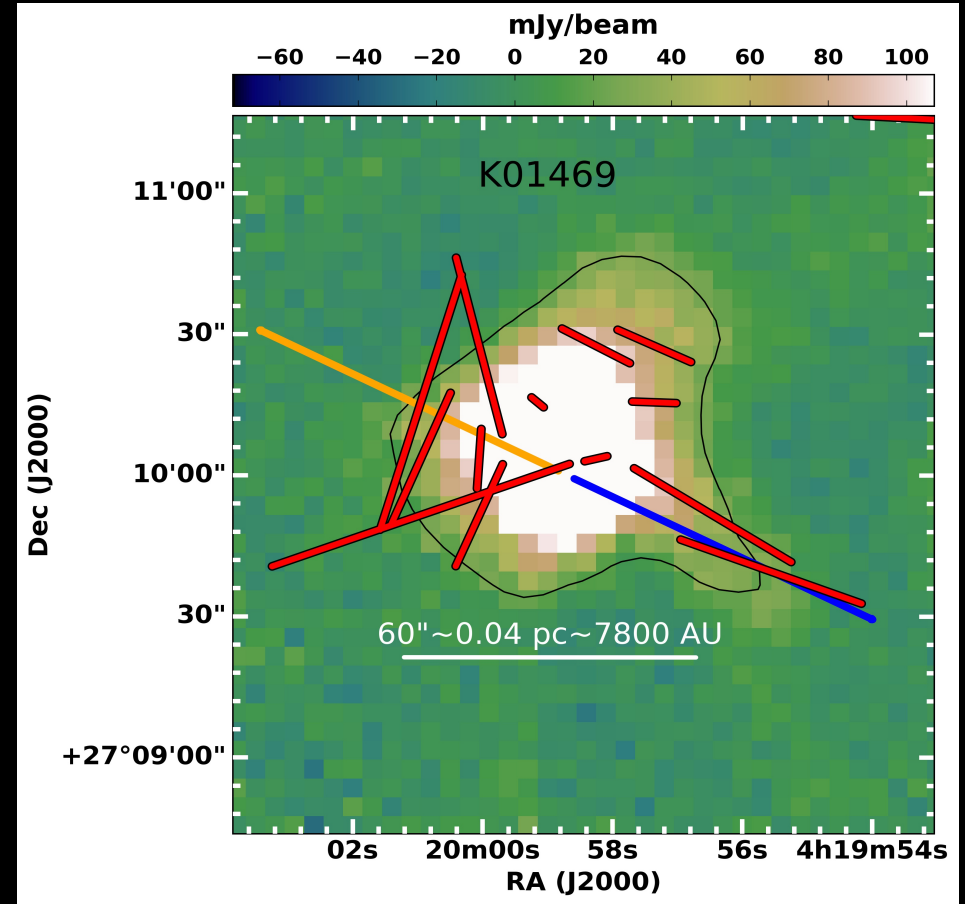
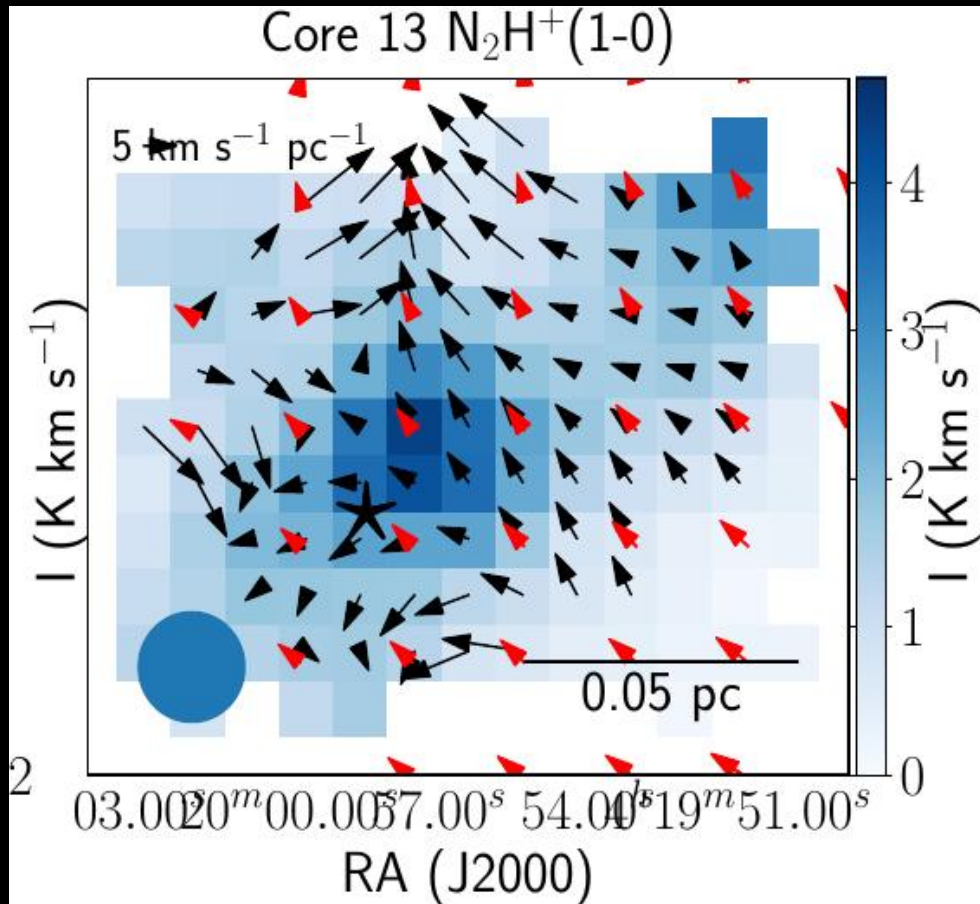
B-fields at larger scales are perpendicular to the filament (5th column; Table below)

At smaller (< 0.1 pc) scales, B-fields follow bimodal distribution: parallel and perpendicular to the filament axis.

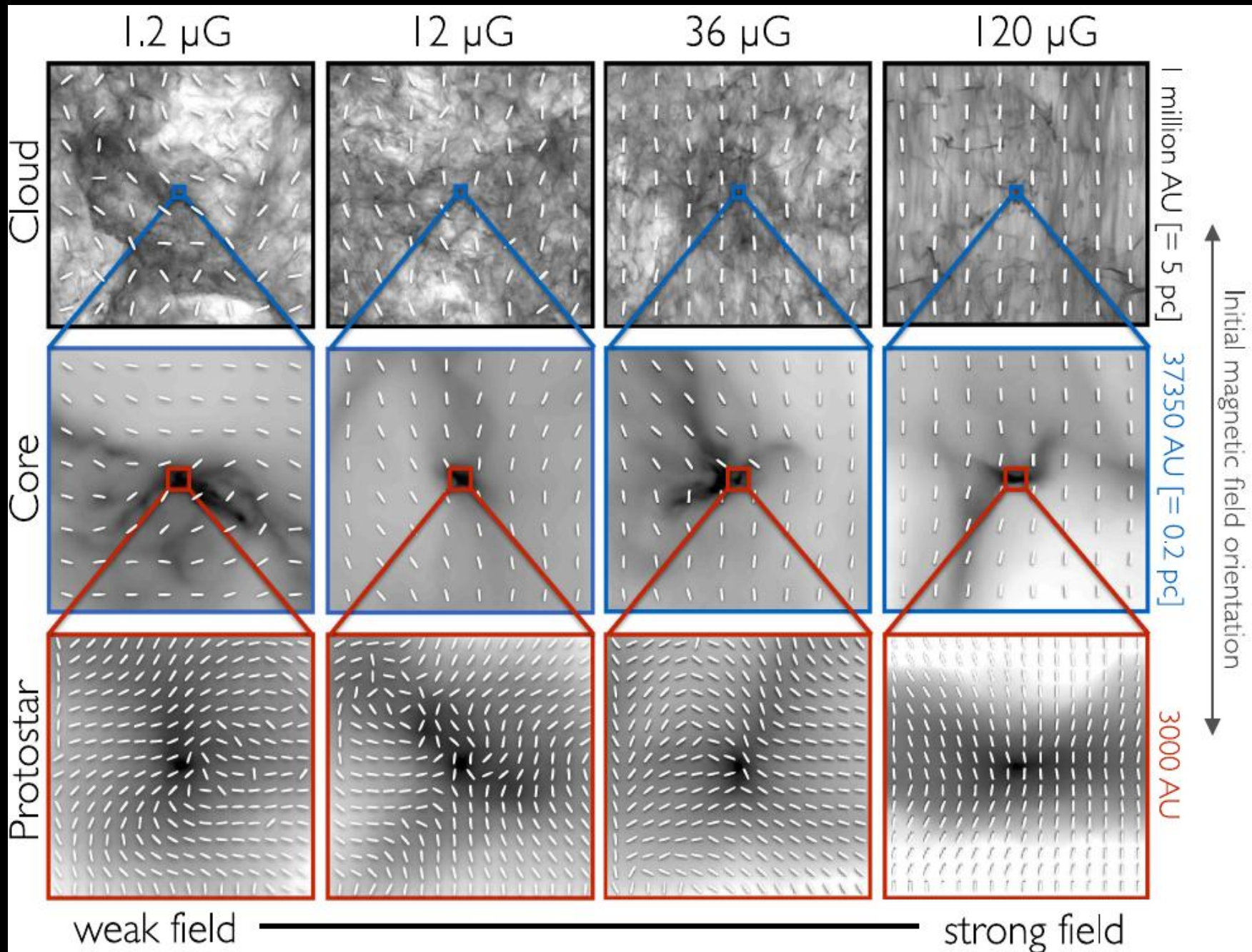
Table 2. Mean B-field orientations based on Optical, NIR, and sub-mm (*Planck*/870 μm) polarization observations.

Wavelength (1) (6)	diameter (arcmin) (2)	No of stars/vectors (3)	Gaussian Mean $\pm\sigma$ ($^\circ$) (4) (relative to filament PA of 135 deg)	Offset PA \ddagger ($^\circ$) (5)
Optical ^a	60	15	29 \pm 14	106
NIR	60	42	37 \pm 17	98
Sub-mm (<i>Planck</i> ^b)	60	445	29 \pm 17	106
Sub-mm (<i>Planck</i> ^c)	16	51	32 \pm 10	103

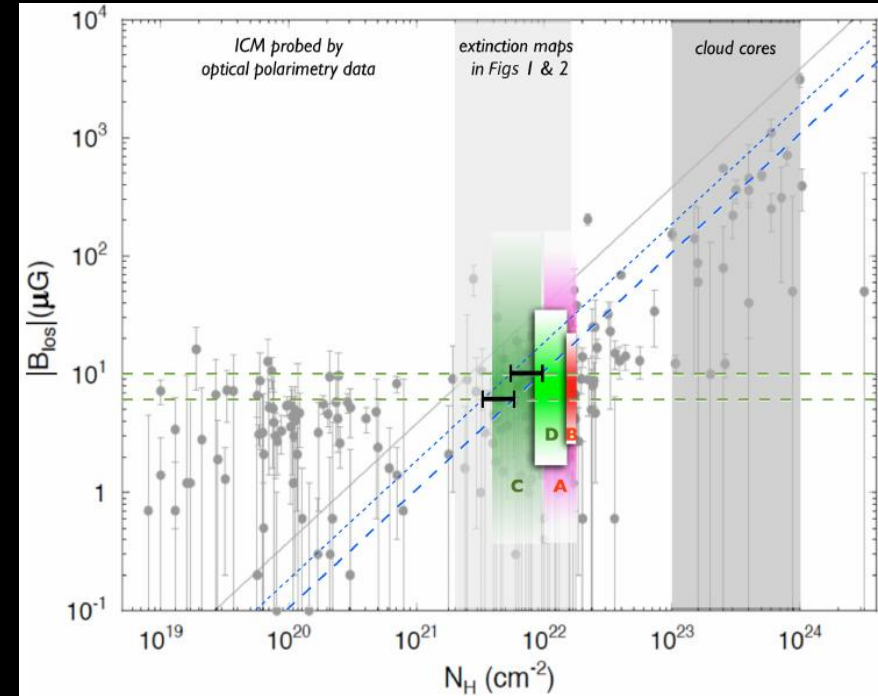
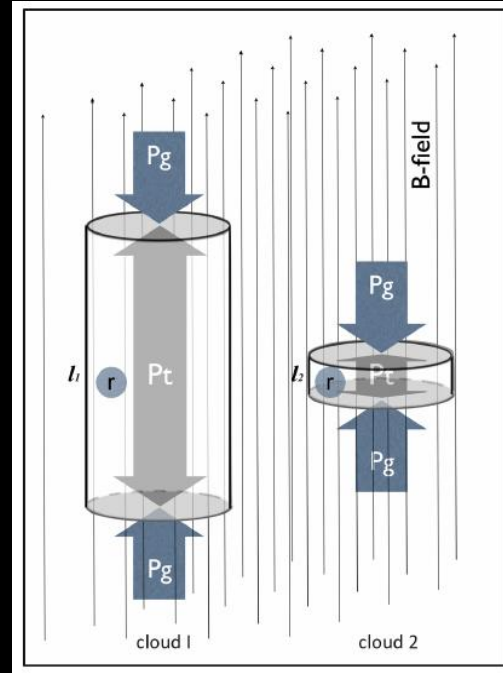
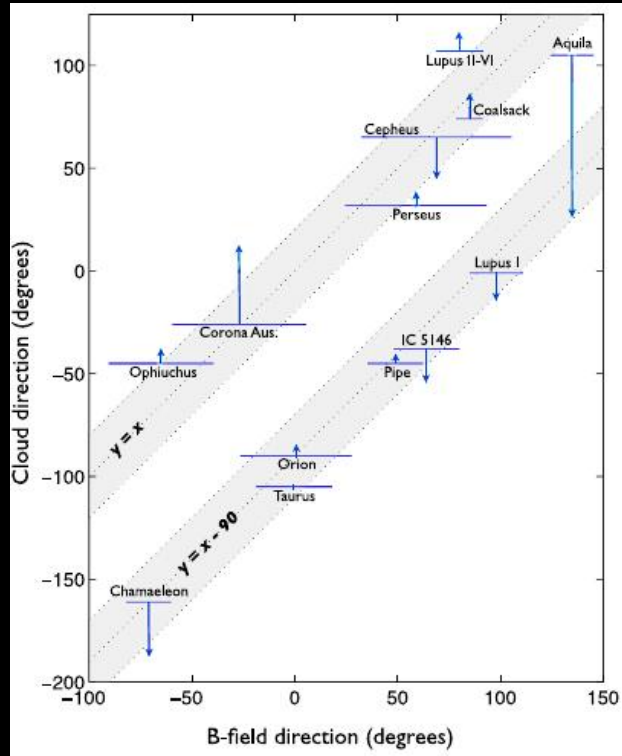
Dominance of other kinematics (rotation, collapse, accretion) in K04169?



Velocity gradients (based on N_2H^+ ; Punanova+ 2018) are seen to be complex nearly following the B-field orientations. Outflows are also seen to be not consistent with the large scale B-fields.



B-field orientation at different scales ranging from several pc to 100's of AU with AREPO simulations with different Alfvén Mac numbers (Hull+ 2017a)

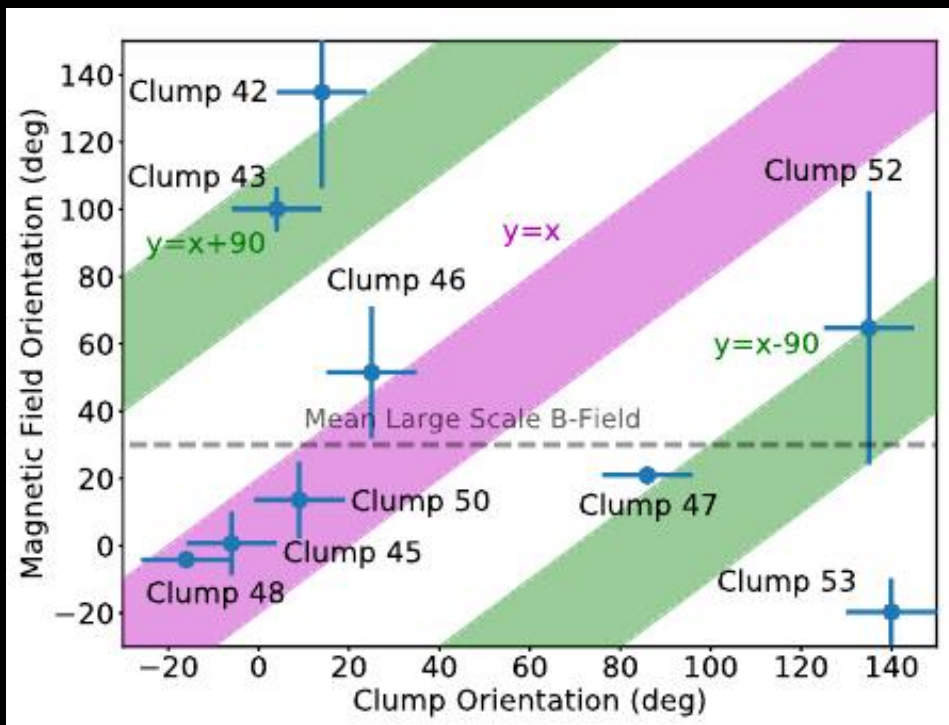


B-fields in intercloud medium (ICM) vs cloud orientation at several pc to 10's of pc scales.

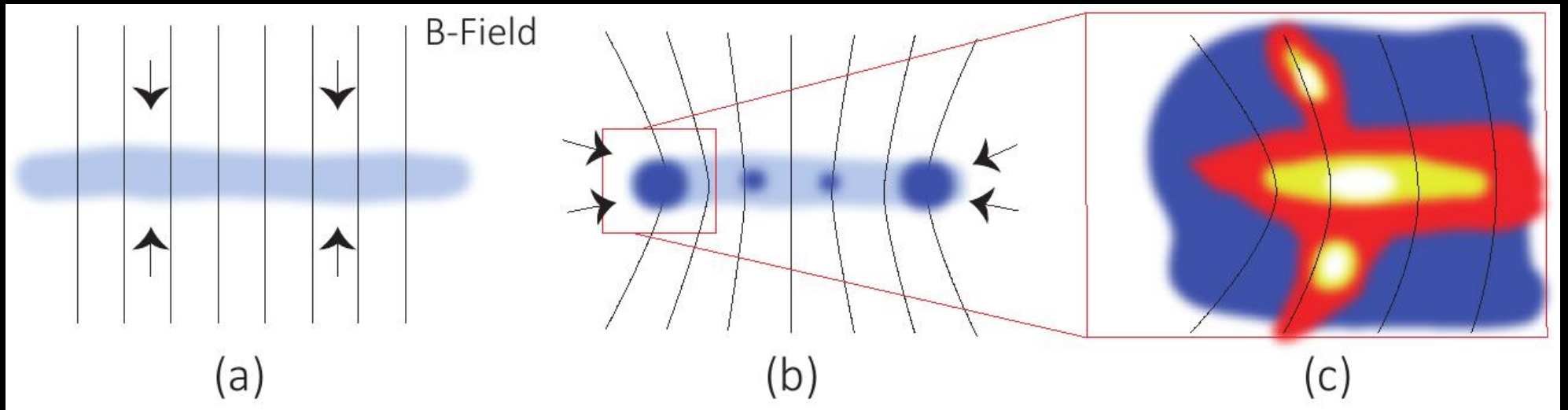
Li+ (2013)

Strong B-fields guide the gravitational contract and channel sub-alfvénic turbulence to produce filaments aligned perpendicular and parallel to the B-fields.

B-field strength remain constant during the cloud accumulation process in the ICM

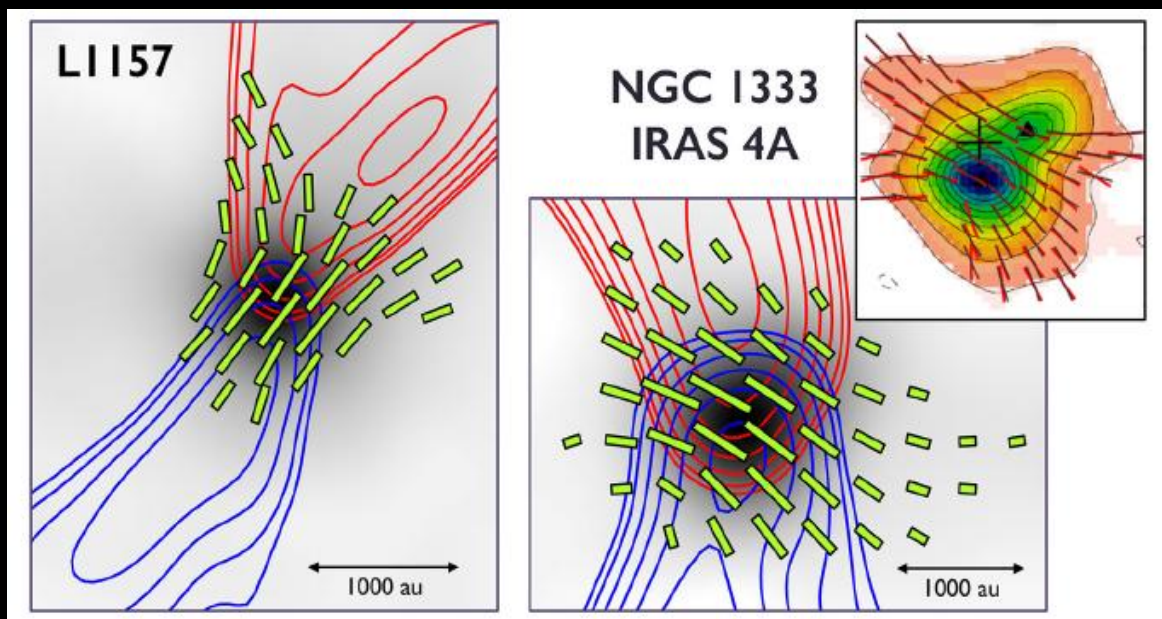


Correlation between B-fields and core structure in hub-filament system of IC5146



Schematic to demonstrate the observed B-fields (Wang+ 2019, towards IC5146, based on JCMTPOL2)

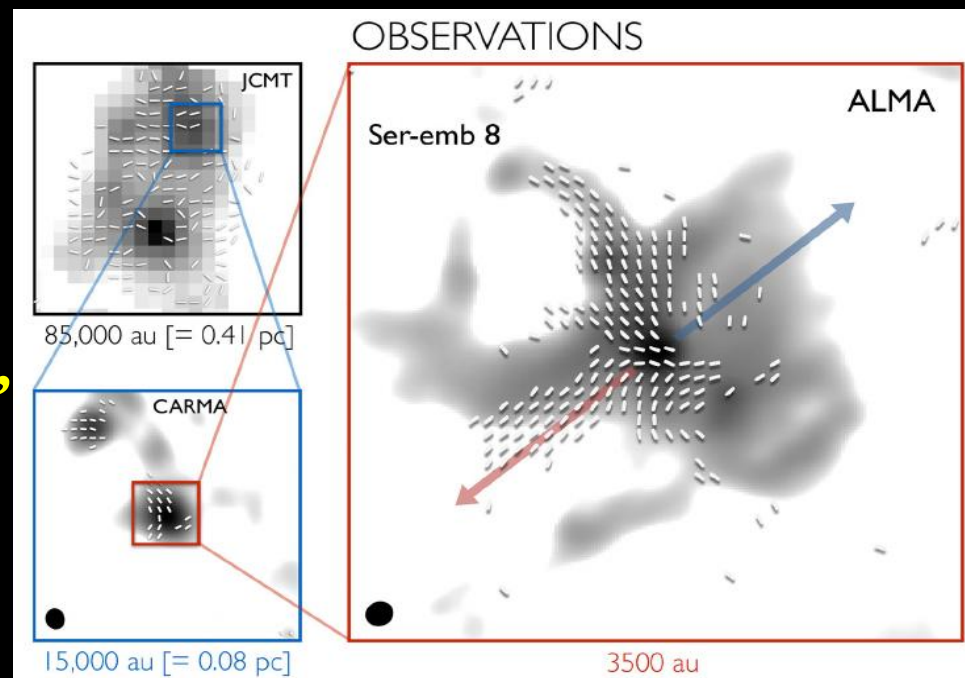
Observational evidences for strong and weak B-field regulated star formation in low-mass cores

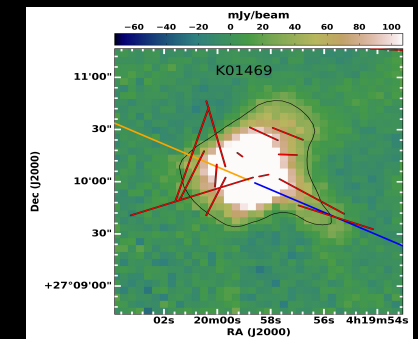
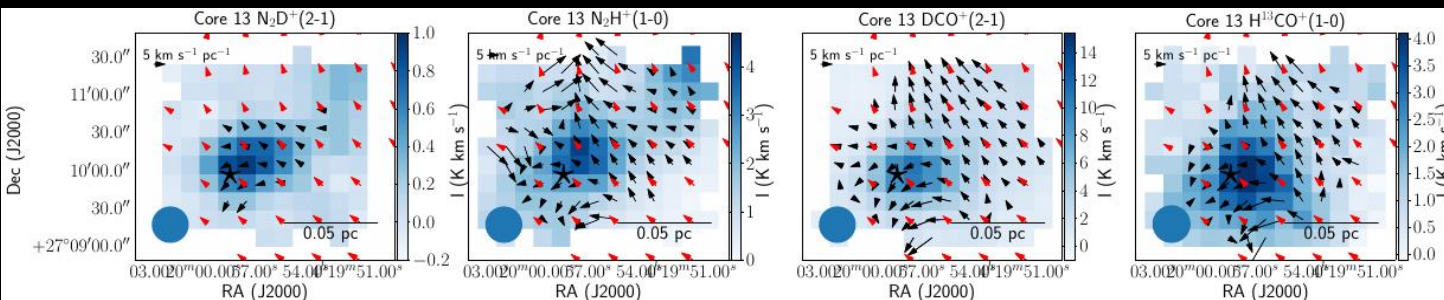
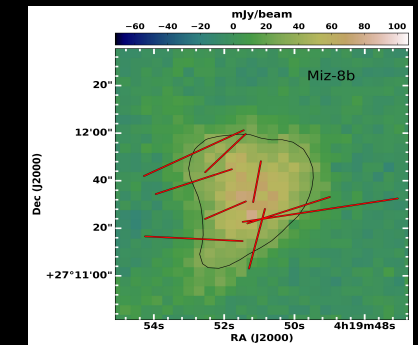
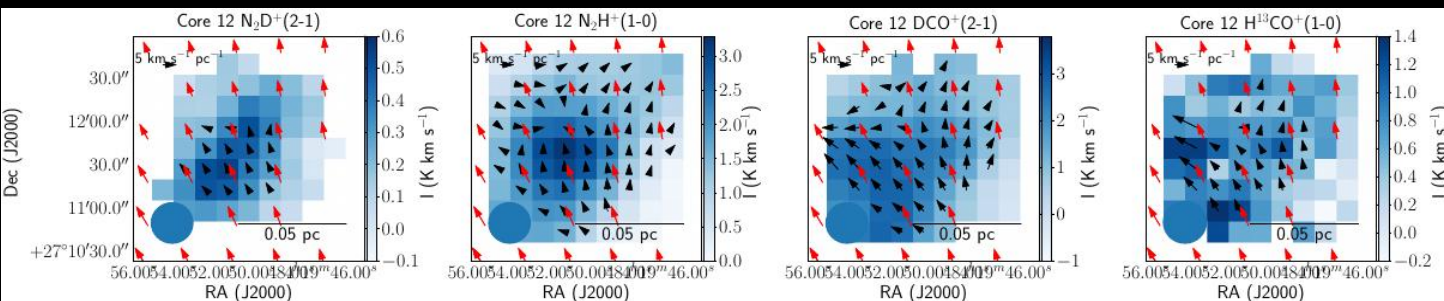
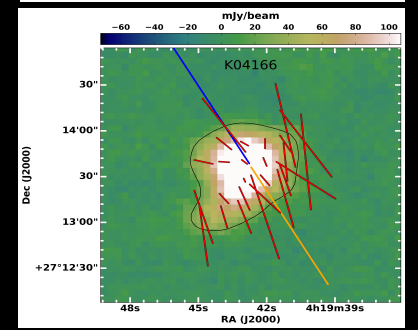
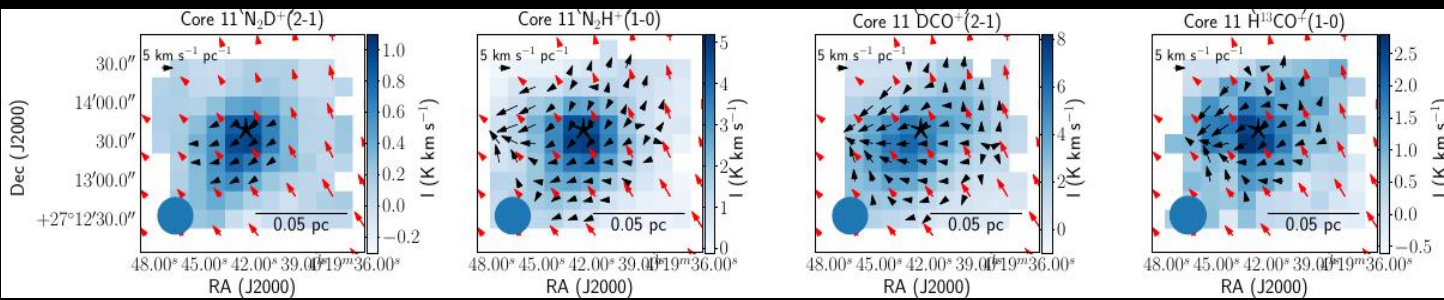
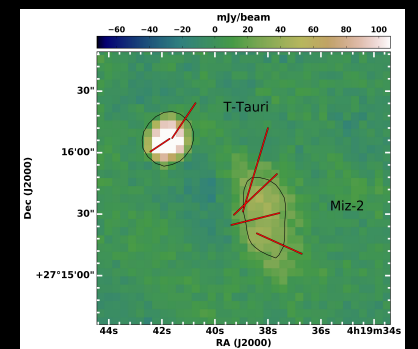
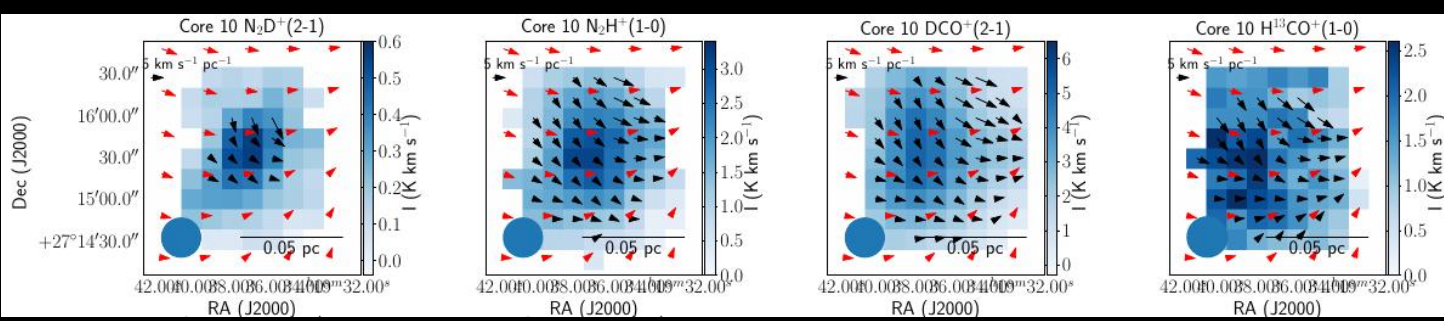


Hourglass shaped B-fields around the Class 0 protostars of L1157 (Hull+ 2014, Stephens+ 2013) and NGC1333 IRAS4A (Girart+ 2006, Hull+ 2014)

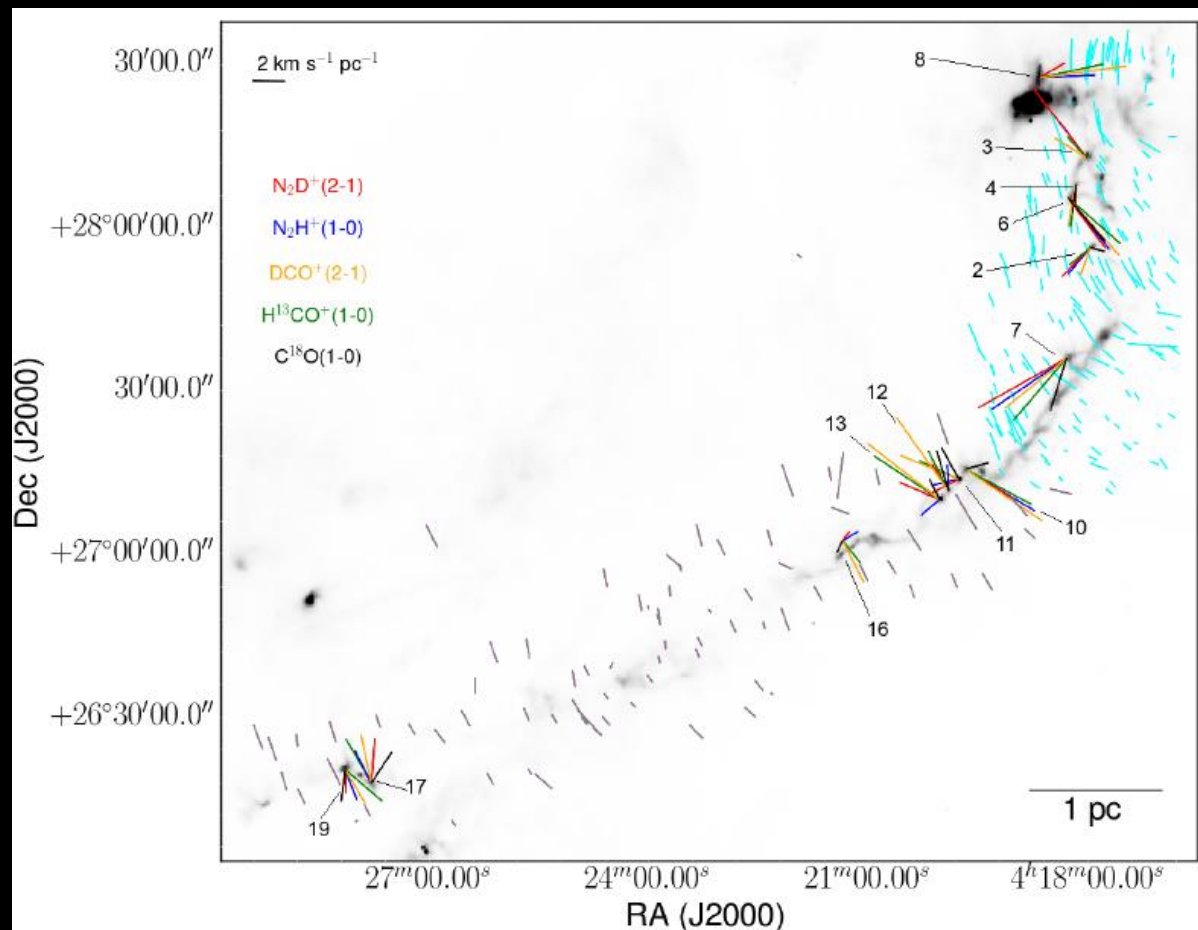
Ordered B-fields at larger scales and chaotic at smaller scales of Class 0 protostar Ser-emb 8 (Matthews+ 1994, Hull+ 2014, Hull+ 2017a)

(Also see Hull+ 2019)





Large scale velocity gradients (red; from C18O data) in Miz2, K04166 and K04169 seem to be aligned with the B-fields. However, local velocity gradients (black) seems complex, in K04169 both larger and local gradients match with each other and also with B-field orientations.



VG orientations seem to be different at different tracers without a preferred orientation

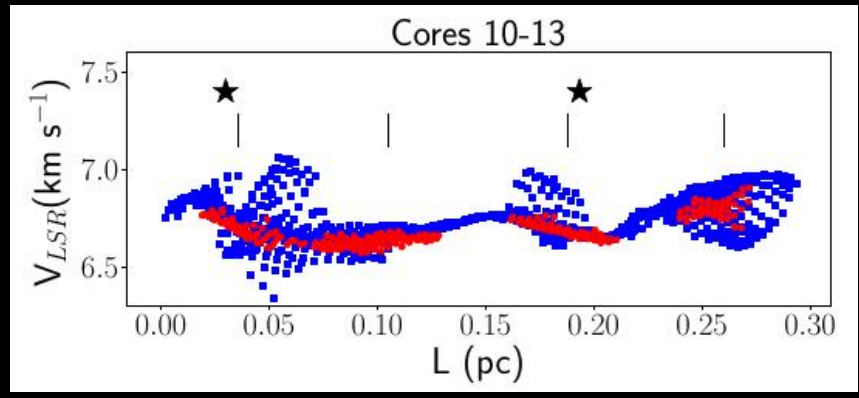
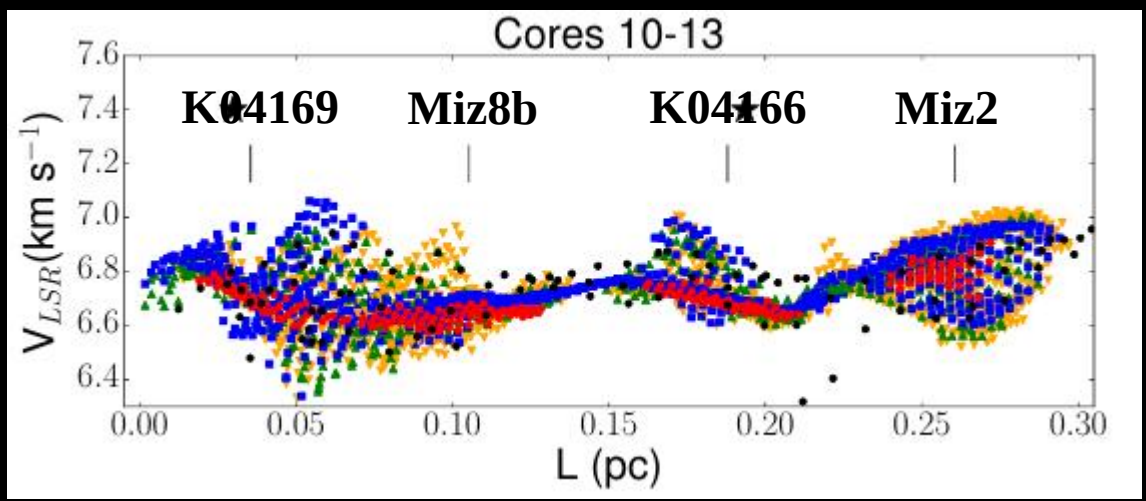
Larger scale gradients (C18O) are in all the cores are not consistent with those of local gradients (N2H+, N2D+, DCO+, H13CO+)

K04169

B-fields at K04169 as well as VGs are complicated

SMA observations: envelope and disk rotations are opposite to each other

Overall V_{lsr} vs length \Rightarrow wave-like pattern – signifying anything?



(All figures are from Punanova+ 2018)

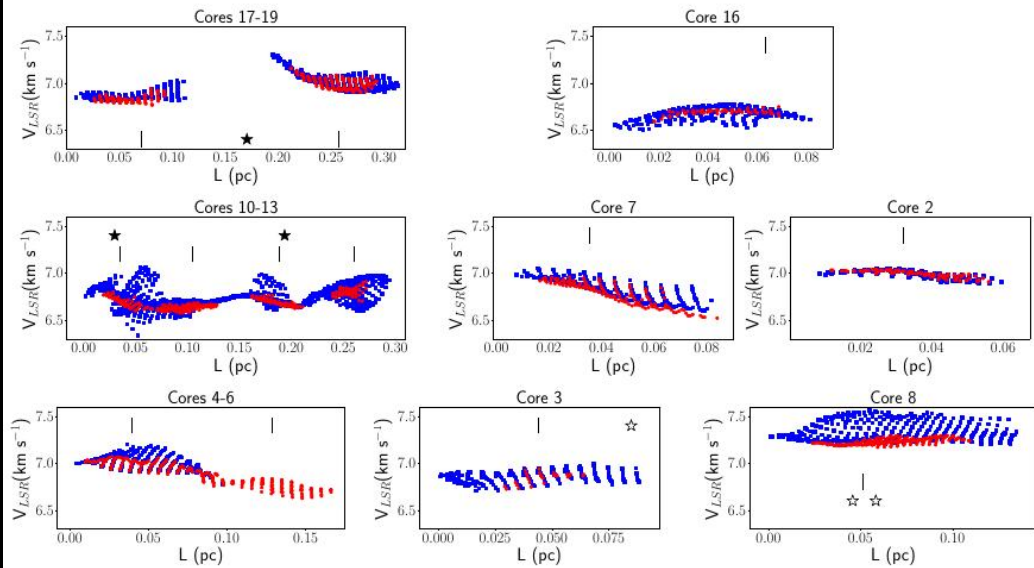


Fig. A.12. V_{LSR} along the filament direction (from core 19 in the south-east to core 8 in the north-west). The transitions are shown with colours: $\text{N}_2\text{D}^+(2-1)$ – red circles and $\text{N}_2\text{H}^+(1-0)$ – blue squares. The vertical bars show the $\text{N}_2\text{H}^+(1-0)$ emission peaks. Stars show the positions of YSOs from [Rebull et al. \(2010\)](#): black stars indicate flat and Class I objects, white stars indicate Class II and III objects.

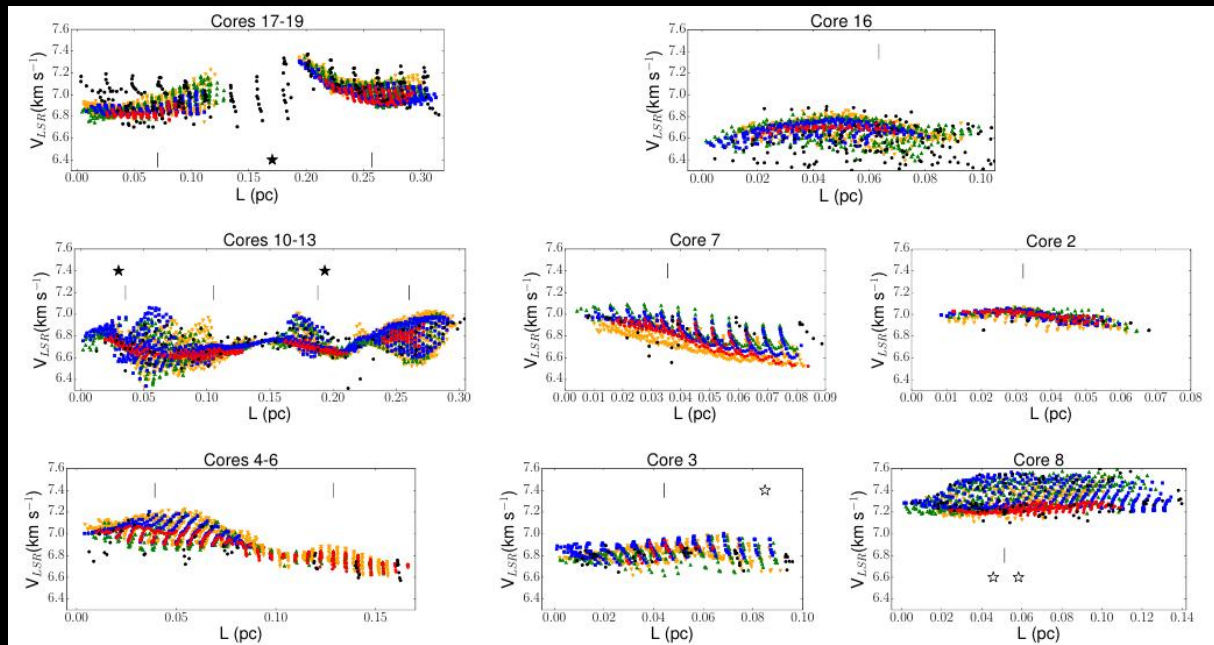


Fig. 5. V_{LSR} along the filament direction (from core 19 in the south-east to core 8 in the north-west). The transitions are shown with colours: $\text{N}_2\text{D}^+(2-1)$ – red circles; $\text{N}_2\text{H}^+(1-0)$ – blue squares; $\text{DCO}^+(2-1)$ – orange flipped triangles; $\text{H}^{13}\text{CO}^+(1-0)$ – green triangles; and $\text{C}^{18}\text{O}(1-0)$ – black circles. The vertical bars show the $\text{N}_2\text{H}^+(1-0)$ emission peaks. Stars show the positions of YSOs from [Rebull et al. \(2010\)](#): black stars indicate flat and Class I objects, white stars indicate Class II and III objects.

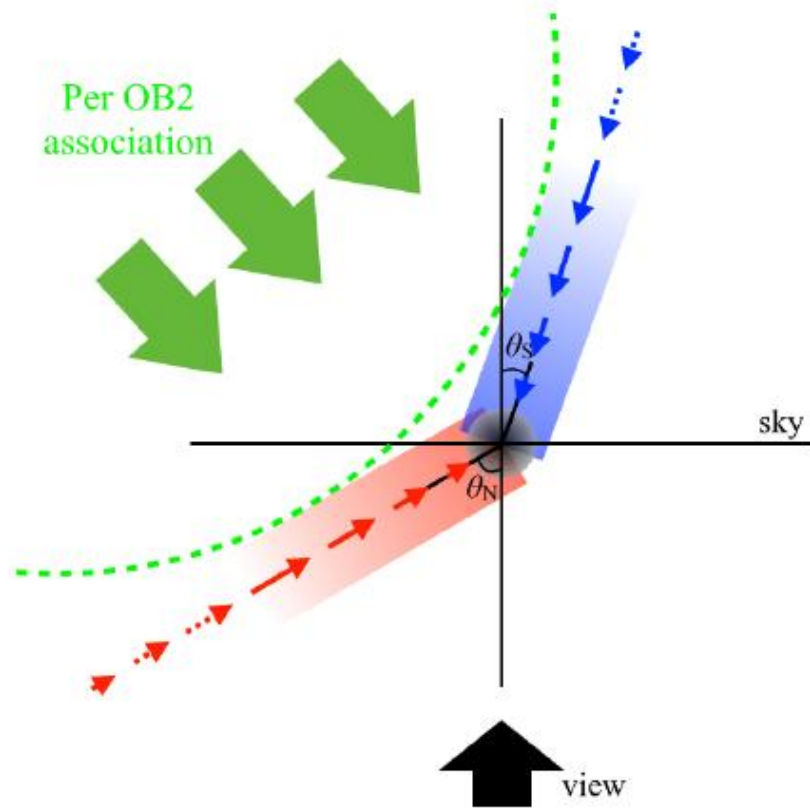


Fig. 9. Schematic picture of the relation between the B211/B213 cloud and Per OB2 association. The black arrows indicate the line of sight. The horizontal line indicate the sky plane. Red and blue arrows indicate the direction of the gas accretion in the northeastern and southwestern sheet components, respectively. Green arrows indicate the direction of the compression by Per OB2 association. θ_N and θ_S are the inclination angles of the northeastern and southwestern sheet components to the line of sight. Red and blue arrows of length scaling quantitatively with the magnitude velocity field indicate the direction of the acceleration flow of ambient cloud material.

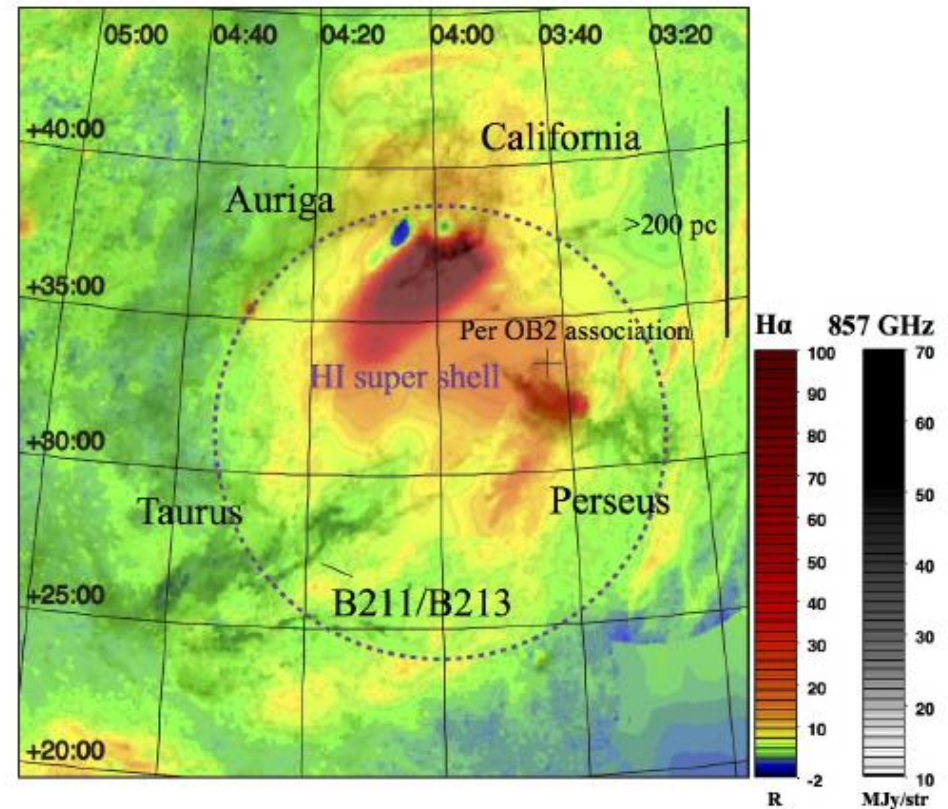
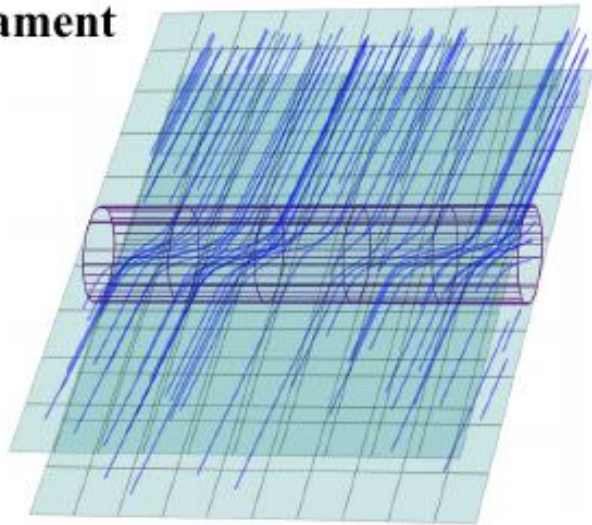


Fig. 10. Distributions of the $H\alpha$ (color; Finkbeiner 2003) and 857 GHz dust (gray; Planck Collaboration I 2014) emission. The units of the $H\alpha$ and 857 GHz maps are R (Rayleigh, $4\pi \times 10^{-4}$ photons $\text{cm}^{-2} \text{s}^{-1} \text{sr}^{-1}$) and $\text{MJy} \text{str}^{-1}$, respectively. The magenta dashed circle indicates a HI supershell (Lim et al. 2013). The diameter of the HI supershell might be >200 pc since the distances to the Taurus and Perseus clouds are 140 and 340 pc, respectively. The distribution of HI emission is shown in Figs. A.4 and A.5. See also Fig. A.6.

Plausible model of the B field in the central filament

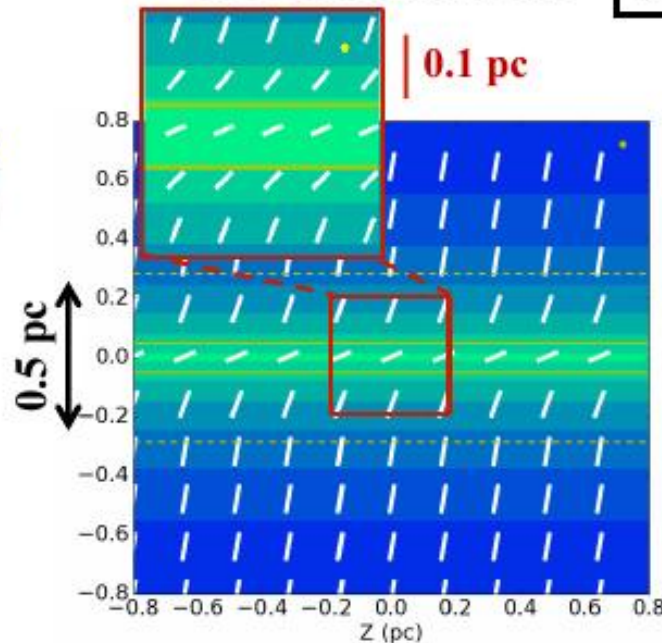


3D view of the model filament system similar to Taurus B211/B213 with B-fields (blue), a cylindrical filament (red lines), and sheet-like background (light green)

B-fields nearly perpendicular to the filament axis, and the axial component got amplified due to gravitational or turbulence compression

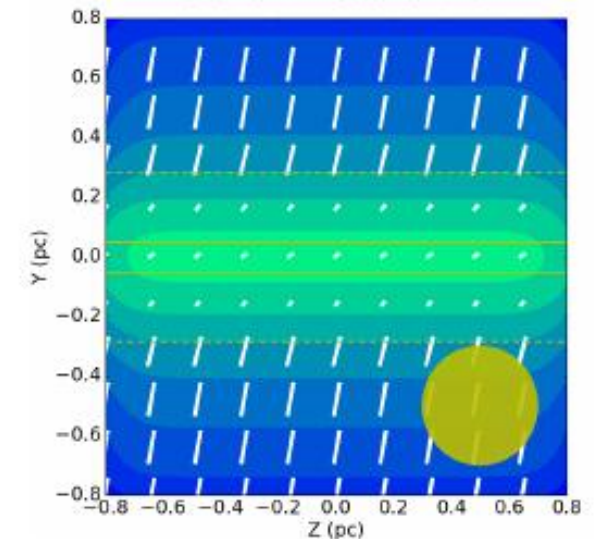
Andre+ 2019 (arXiv:1905.03520)

SPICA resolution



Synthetic polarization maps

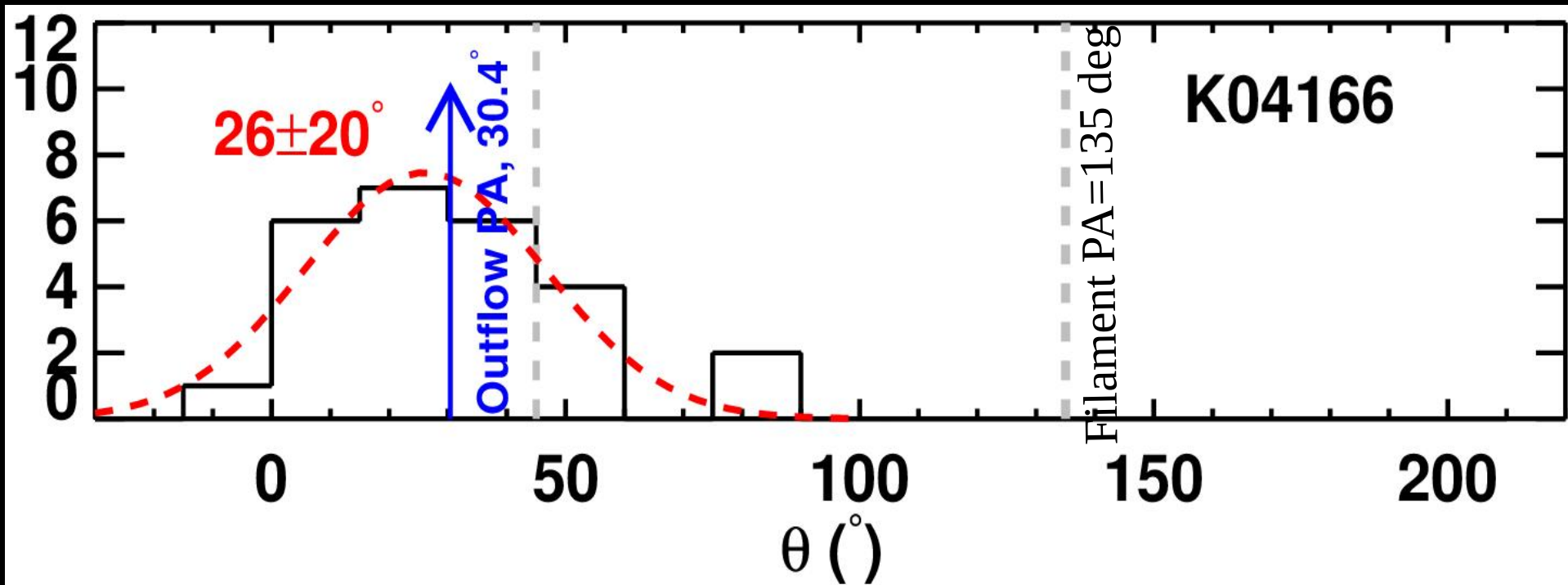
Planck resolution



Synthetic B-field map expected at the resolution of $\sim 20''$ of SPICA-POL/B-BOP at 200 micron according to the model.

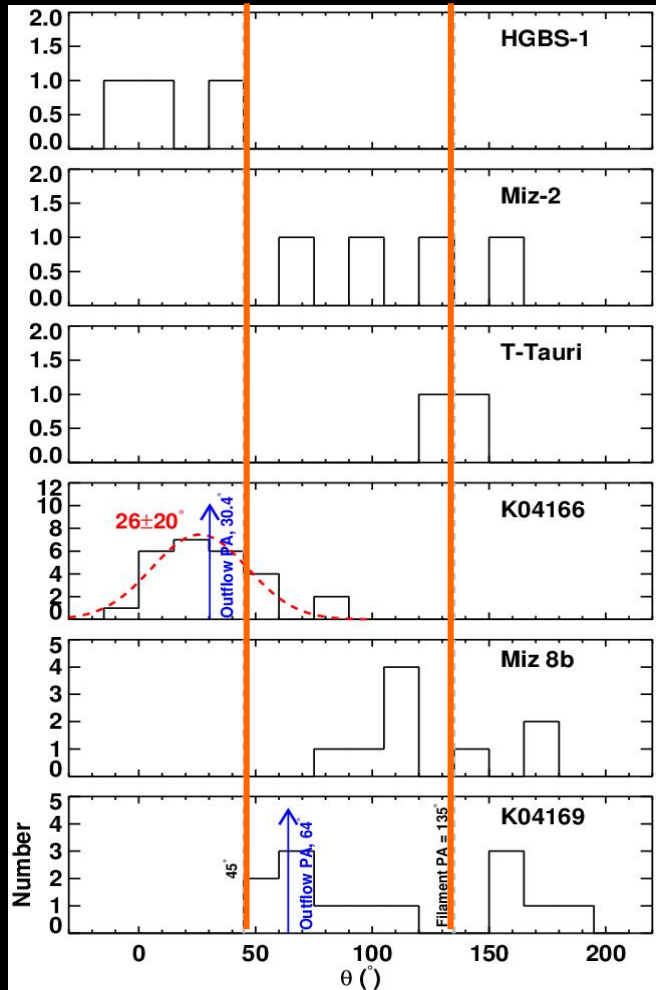
Synthetic B-field map expected at the 5' resolution with *Planck* as per the model.

Our results from JCMT-POL2: B-fields in more evolved protostellar cores follow those at larger scales, while in the prestellar cores they are in parallel configuration.



Distribution of B-fields

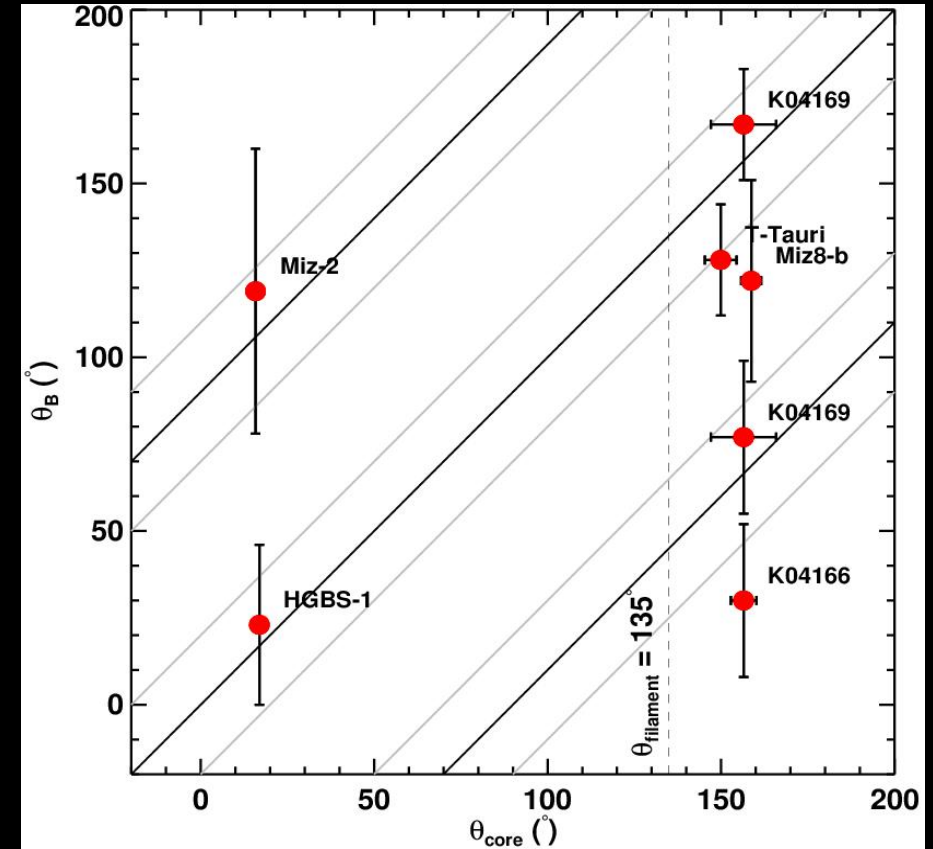
B-fields vs PA of filament



Miz-2, T-Tauri, Miz8-b, K04169 have the B-fields components parallel to the filament

HGBS-1, K04166, K04169 have B-fields coherent with large scale B-fields (perpendicular to the filament)

B-fields vs PAs of cores

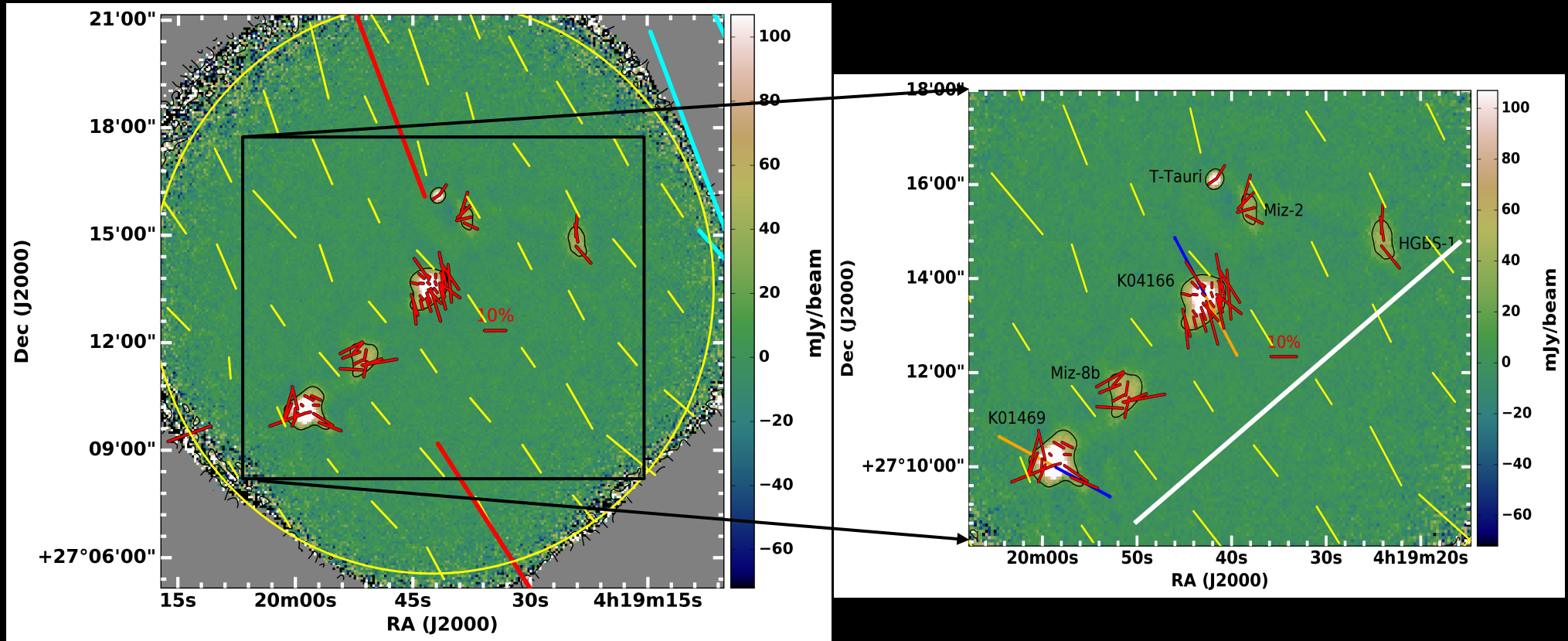


Core orientations are either parallel or perpendicular to the mean B-field geometries

Table 3. Weighted mean orientation of B-fields of the seven cores of B213 based on JCMT/SCUBAPOL2.

Name of the core	No. of vectors	Weighted mean \pm error ($^{\circ}$)	standard deviation ($^{\circ}$)
HGBS-1	3	23 ± 6	23
Miz-2	4	119 ± 5	41
T Tauri	2	128 ± 6	16
K04166 [*]	26	30 ± 1	22
Miz-8b	9	122 ± 3	29
K04169 ^a	8	77 ± 4	22
K04169 ^b	5	167 ± 4	16

Comparison between B-fields at larger and smaller scales



Absence of coherency between Optical/NIR/Planck and JCMT/SCUBAPOL2 B-fields. However, B-fields in HGBS-1, K01466, k04169 are coherent with large scales B-fields, while in Miz-2, Miz-8b, and T-Tauri they are perpendicular.